KRITTIKA SUMMER PROJECTS 2023

Exploring the Radio Sky

Atreyi Dasgupta

Pngtree

KRITTIKA SUMMER PROJECTS 2023

Exploring the Radio Sky

Atreyi Dasgupta[1]

[1]Birla Institute of Technology And Science Pilani (BITS), Hyderabad Campus

Copyright © 2023 Krittika IITB
PUBLISHED BY KRITTIKA: THE ASTRONOMY CLUB OF IIT BOMBAY
GITHUB.COM/KRITTIKAIITB
First Release, September 2023

Abstract

We aim to develop a proficient understanding of radio astronomy by exploring its foundational concepts and applying them to analyze data collected from radio telescopes using CASA (Common Astronomy Software Applications) software. The project focuses on hands-on learning, delving into the principles underlying radio astronomy and utilizing CASA to process and interpret data obtained from radio telescopes. The results are further effectively understood by appropriate plots. This report provides a comprehensive learning experience that enables participants to gain proficiency in the fundamental aspects of radio astronomy and its data analysis techniques, with a specific focus on CASA software as a powerful tool for radio astronomical research. We have utilized MCMC as a powerful data sampler, enabling us to explore complex models and extract reliable parameter estimates. Additionally, we investigated fast radio bursts (FRBs) and their dispersion measure (DM) values, which provide valuable information about the intervening medium and the sources of these energetic bursts.

Contents

I Part One

1 Multi wavelength Astronomy 7

1.1 Electromagnetic Spectrum 7

1.2 Galaxies in different wavelengths 8

1.2.1 Whirlpool Galaxy 9

1.2.2 Sunflower Galaxy 9

1.2.3 Needle Galaxy 9

1.2.4 UGC00595 10

2 Sky Coordinate System 11

2.1 Right Ascension and Declination 11

2.2 Observer-Centered Definitions 11

3 Jet afterglow lightcurve 15

3.1 Introduction 15

3.2 Plots 16

4 MEASURES OF THE AMOUNT OF RADIATION 19

4.1 Radiation Physics definitions 19

5 Cosmic Microwave Background 21

5.1 Planck's Function 22

5.2 Curve Fitting 22

6 Hydrogen 21 cm Line 23
6.1 Introduction 23
6.2 Galaxy Rotation Curve 23

7 Radio Telescopes 25
7.1 RADIO TELESCOPE REFLECTORS, ANTENNAS, AND FEEDS 25
7.1.1 Primary Reflectors 25
7.1.2 Beam Pattern 25
7.1.3 Feeds and Primary Reflector Illumination 26
7.1.4 Surface errors 26
7.2 Noise, Noise Temperature and Antenna Temperature 26

II Part Two

8 Radio Astronomy Observing Basics 31
8.1 Two element interferometer 31
8.2 Observation of a single point source 32
8.3 Visibility equation for a general extended source 32

9 Common Astronomy Software Applications 35
9.1 CASA 35
9.2 TW Hydra 35
9.2.1 Getting information of the object 36
9.2.2 Interactive Cleaning of the image 36
9.2.3 Non-interactive clean 38
9.2.4 Primary Beam Correction 41
9.2.5 Statistics 42
9.3 Supernova Remnant 3C 391 42
9.3.1 Imaging 43
9.3.2 Multi-scale Mosaic Clean 43
9.3.3 Image Analysis 45

10 Markov-Chain Monte Carlo (MCMC) 47
10.0.1 Fitting the lightcurve of GW170817 49

11 Fast Radio Bursts 53

Part One

1 **Multi wavelength Astronomy** 7
1.1 Electromagnetic Spectrum
1.2 Galaxies in different wavelengths

2 **Sky Coordinate System** 11
2.1 Right Ascension and Declination
2.2 Observer-Centered Definitions

3 **Jet afterglow lightcurve** 15
3.1 Introduction
3.2 Plots

4 **MEASURES OF THE AMOUNT OF RADIATION** 19
4.1 Radiation Physics definitions

5 **Cosmic Microwave Background** 21
5.1 Planck's Function
5.2 Curve Fitting

6 **Hydrogen 21 cm Line** 23
6.1 Introduction
6.2 Galaxy Rotation Curve

7 **Radio Telescopes** 25
7.1 RADIO TELESCOPE REFLECTORS, ANTENNAS, AND FEEDS
7.2 Noise, Noise Temperature and Antenna Temperature

1. Multi wavelength Astronomy

1.1 Electromagnetic Spectrum

We can only see a small segment of the night sky, what visible light allows us to see. Multi-wavelength Astronomy is about getting the complete picture. The electromagnetic spectrum encompasses the entire range of light, incorporating a diverse array of colors we typically perceive. Within this spectrum, we encounter various types of radiation, including gamma rays, X-rays, ultraviolet, visible light, infrared, microwaves, and radio waves. The key distinguishing factor among these types of radiation lies in their characteristic wavelength or frequency. As we move from gamma rays to radio waves, wavelengths increase while frequencies decrease. Remarkably, all these forms of radiation travel at a uniform speed known as the speed of light, which amounts to approximately 186,000 miles per second (or 300 million meters per second).

Studying the Universe across the vast expanse of the electromagnetic spectrum grants us a more comprehensive understanding of celestial objects. Each segment of the spectrum offers invaluable and distinct information. X-rays and gamma rays unveil insights into energetic phenomena like black holes, supernova remnants, hot gas, and neutron stars. Ultraviolet light exposes hot stars and quasars, while visible light illuminates warmer stars, planets, nebulae, and galaxies. Infrared observations unveil cool stars, regions of star formation, dusty cosmic expanses, and the heart of our galaxy. Radio radiation allows us to explore cold molecular clouds and reveals the remnants of the cosmic background radiation, a remnant from the early stages of the universe known as the Big Bang.

The study of celestial objects unveils a rich tapestry of radiations across the vast expanse of the electromagnetic spectrum. This spectrum encompasses an array of emissions, each carrying unique insights into the nature of the cosmos. At one extreme, we find gamma rays, the most energetic form of radiation, originating from processes such as supernovae and black hole interactions. Moving down the spectrum, we encounter X-rays, which reveal the presence of hot gas and compact stellar remnants. Ultraviolet radiation unveils the secrets of hot stars and quasars, while visible light provides a window into the warmer stars, planets, nebulae, and galaxies that populate our universe. Infrared emissions expose cool stars, regions of star birth, dusty cosmic expanses, and the core of our galaxy. Microwaves offer glimpses into the universe's faint whispers, including the remnants of the Big Bang and the cosmic microwave background radiation. Lastly, radio waves enable the study of cold molecular clouds and the mapping of celestial radio sources. Together, the diverse range of radiations spanning the electromagnetic spectrum allows us to piece together a more comprehensive understanding of the celestial tapestry that surrounds us.

1.2 Galaxies in different wavelengths

We will take three galaxies: namely, Whirlpool Galaxy, Sunflower Galaxy and Needle Galaxy.

To acquire the necessary images, we will utilize the CIRADA image cutout web service. This service enables us to obtain optical, infrared, and radio images of all three galaxies. The optical images will provide us with a visual representation of the galaxies, showcasing their intricate spiral arms, bright stellar clusters, and other prominent features. Infrared images, on the other hand, will reveal cooler regions of star formation, dust-obscured regions, and possibly hidden stellar populations. Lastly, radio images will allow us to detect and study radio-emitting sources within the galaxies, such as molecular clouds and radio jets from active galactic nuclei.

Different wavelengths reveal distinct aspects of galaxies. Optical observations provide information about the distribution of stars and their colors. Infrared observations penetrate dust clouds, allowing us to study cooler regions, star formation, and obscured objects. Radio observations help us detect neutral hydrogen gas and map out large-scale structures. By combining data from multiple wavelengths, we obtain a more complete and detailed picture of the galaxy.

For the following set of images, we obtain the images using the CIRADA (2) image cutout web service. We will mainly see optical, infrared and radio images of all the three galaxies.

1.2.1 Whirlpool Galaxy

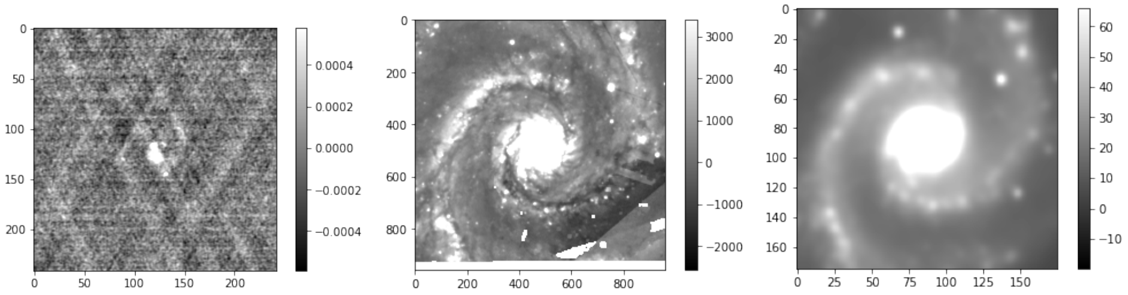

(a) Radio (b) Optical (c) Infrared

Figure 1.1: Different wavelength images of Whirpool Galaxy

1.2.2 Sunflower Galaxy

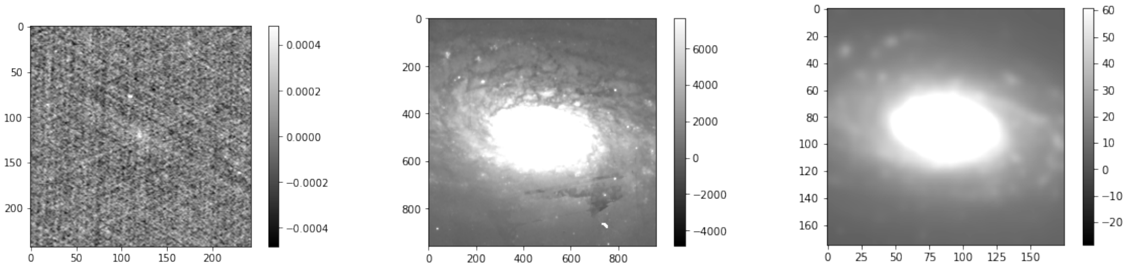

(a) Radio (b) Optical (c) Infrared

Figure 1.2: Different wavelength images of Sunflower Galaxy

1.2.3 Needle Galaxy

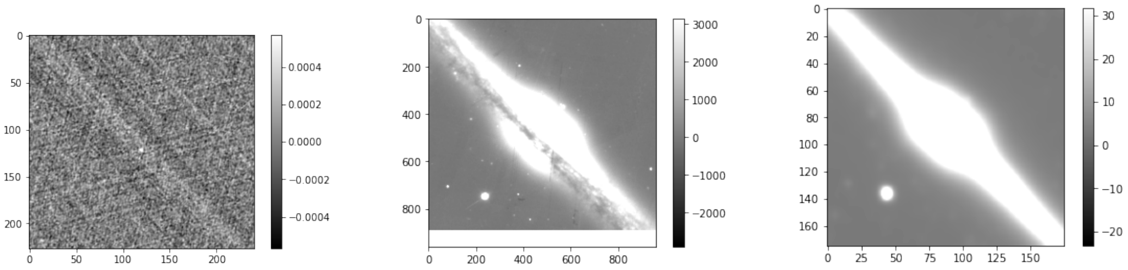

(a) Radio (b) Optical (c) Infrared

Figure 1.3: Different wavelength images of Needle Galaxy

Now, we will observe a galaxy which has good radio frequencies, to get good results, we will see galaxies in the Jets and Lobes section.

1.2.4 UGC00595

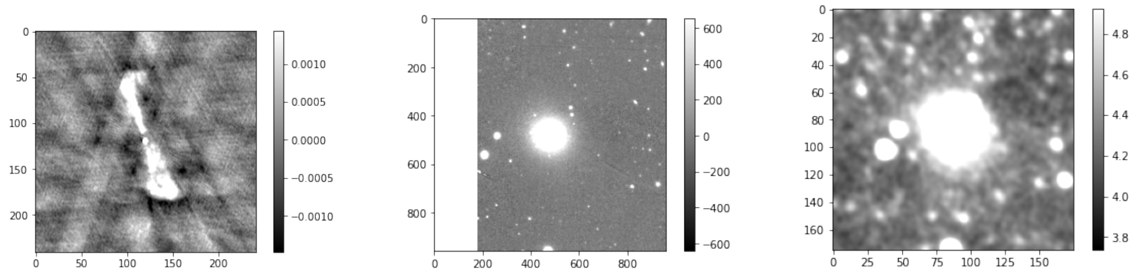
0
50
100
150
200
0.0010
0.0005
0.0000
−0.0005
−0.0010
0
200
400
600
800
600
400
200
0
−200
−400
−600
0
20
40
60
80
100
120
140
160
0
25
50
75
100
125
150
4.8
4.6
4.4
4.2
4.0
3.8

(a) Radio (b) Optical (c) Infrared

Figure 1.4: Different wavelength images of UGC00595 Galaxy

2. Sky Coordinate System

2.1 Right Ascension and Declination

To find and observe objects in the sky, we need an established and consistent system of defining their location, that is, a coordinate system. To us, on Earth, the surrounding sky appears like a spherical shell—we can see the directions to objects but we do not know their distances. Since Earth, also, is (roughly) a sphere, and we have an established coordinate system for it, the sky coordinate system that is set up is basically the same construct. Therefore, picture a globe of the sky, called the celestial sphere, with a globe of Earth at its center.

Extensions of the lines of longitude on Earth produce similar lines on the sky, which we call lines of right ascension (RA), often represented by the Greek letter α. Extensions of the lines of latitude make lines on the sky called declination (Dec), represented by the Greek letter δ.

2.2 Observer-Centered Definitions

(6)

1. *Horizon*: This defines the limit of what parts of the sky you can see at any particular moment. It is due to the ground and structures on Earth blocking your view of the sky. If Earth were transparent, you could also view the sky below your feet by looking through Earth. Since Earth is not transparent, you cannot see this part of the sky, because it is below your horizon.

2. *Zenith*: This is the point in the sky directly overhead. Since the sky rotates continuously, this point on the celestial sphere continually changes, unless you are standing at either the North or the South Pole.

3. *Altitude or elevation*: These are synonyms for the angular height of an object above your horizon at any given moment. When a star is on your horizon (so that it is either just rising or just setting), its altitude, or elevation, is 0°, and when it is directly overhead—at the zenith—its altitude, or elevation, is 90°. Keep in mind that this is an angle, not a physical distance. Figure 1.9 displays the altitude angle of a star.

4. *Azimuth*: This is the angular position perpendicular to the altitude, and is defined as the angular position of an object along the horizon relative to due north. If the object is located to the north of the zenith, its azimuth is 0°. If it is located to the south of the zenith, it has an azimuth of 180°. An azimuth of +90° is due east and 270° is due west. All observers will see the same RA and Dec for an astronomical object, but the altitude and azimuth for the object will be different for observers at different locations, and indeed, even for the same observer, at different times of the day.

5. *Meridian*: This is the line of RA that runs through your zenith. Equivalently, it is the line in the sky that runs through both your zenith and the celestial poles. Consider the following. As Earth rotates, you will see the stars move across the sky from east to west. Consider, for a moment, just the stars that are at the same Dec as your latitude; these are the stars that will pass directly overhead (i.e., through the zenith) on their trek westward. The moment that one of these stars is at the zenith is when it is highest in the sky (i.e., when it reaches its maximum elevation). Stars that are at different Decs will never pass directly overhead because the point directly overhead must have the same Dec as your latitude (by definition of Dec). All stars, regardless of their Dec, will be highest in the sky during the moment when they cross your meridian. This is important because it is the best time to observe a particular object, and it also defines the midpoint of the time that an object is visible above the horizon (i.e., the moment in time halfway between rising and setting).

6. *Transit*: (verb) means to pass through the meridian.

7. *Hour angle (HA)*: An object's HA is the amount of time (in hours) since the object transited. For example, if the object is currently at the meridian, its HA at that moment is 0. If the object transited 1 h ago, it has an HA of +1 h, and if it will transit in two and a half hours, then its HA is –2.5 h.

8. *Local sidereal time (LST)*: This is defined as the RA of the meridian. While you are observing, the computer will keep track of your LST. This number is useful to help you keep track of what objects are transiting or when a particular object will transit. You must know an object's RA (as given in a catalog) in order to observe it. In addition, if you also know the LST, you can calculate the object's HA from : HA = LST - RA.

9. *Universal time (UT):* This is the solar time in Greenwich, England (i.e., the time on the clock where the longitude is 0°). This is useful for marking the exact time of an observation or an event. One does not need to know, then, from what time zone the observation was made. It defines a time that is the same

for everyone on Earth. Universal time is particularly useful for situations in which the different time zones can cause confusion. Airlines, for example, actually schedule their flights using Universal time, but translate to local time for the customers.

3. Jet afterglow lightcurve

3.1 Introduction

For the first time, scientists have directly detected gravitational waves — ripples in space-time — in addition to light from the spectacular collision of two neutron stars. This marks the first time that a cosmic event has been viewed in both gravitational waves and light.

The discovery was made using the U.S.-based Laser Interferometer Gravitational-Wave Observatory (LIGO) (1); the Europe-based Virgo detector; and some 70 ground- and space-based observatories.

Neutron stars are the smallest, densest stars known to exist and are formed when massive stars explode in supernovas. As these neutron stars spiraled together, they emitted gravitational waves that were detectable for about 100 seconds; when they collided, a flash of light in the form of gamma rays was emitted and seen on Earth about two seconds after the gravitational waves. In the days and weeks following the smashup, other forms of light, or electromagnetic radiation including X-ray, ultraviolet, optical, infrared, and radio waves were detected. The observations have given astronomers an unprecedented opportunity to probe a collision of two neutron stars.

We used the data for the non-thermal emission from this source that spans across all frequency bands following a single spectral index of $F_\nu \propto \nu^{-0.584}$. The quantity F_ν is the flux density, which measures the amount of energy incident on the detector per unit area of the detector, an indicator of the brightness of the source. A lightcurve is this flux density represented as a function of time.

3.2 Plots

We plot the lightcurve choosing all the VLA 3 GHz data points.

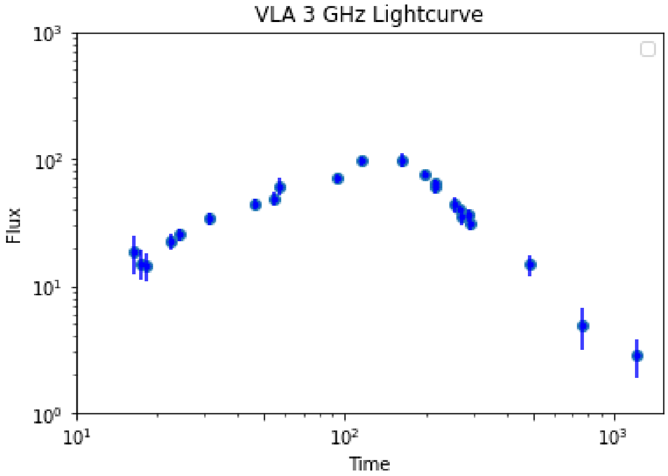

Figure 3.1: **Time vs. Flux Density at 3GHz:** *The plot shows the time evolution of the flux density observed by the VLA telescope at a frequency of 3GHz.The error bars indicate the uncertainties associated with each flux density measurement.*

We choose another instrument, say Chandra, an X-ray instrument that has observations of our source at 2.41 × 10^{17} Hz.

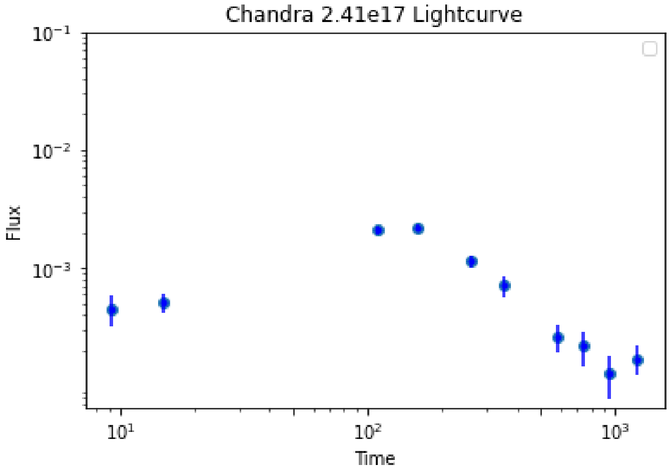

Figure 3.2: **Time vs. Flux Density at 2.41 × 10^{17} Hz:** *The plot shows the time evolution of the flux density observed by the Chandra telescope at a frequency of 2.41 × 10^{17} Hz.The error bars indicate the uncertainties associated with each flux density measurement*

The plot above is the Chandra Lightcurve at 2.41 x 10^{17} Hz.

We Scale the Chandra flux densities to 3 GHz using $F_\nu \propto \nu^{-0.584}$ and then we overplot the Chandra data points over the VLA 3 GHz data points that we just plotted.

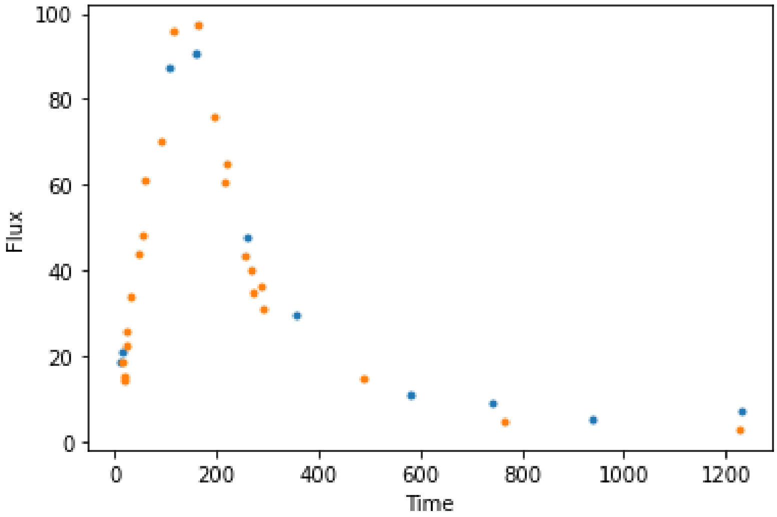

Figure 3.3: **Comparison of VLA and Chandra Observations:** *The plot showcases the VLA 3 GHz data points (previously plotted) and overlays the Chandra data points, which have been scaled to 3 GHz using the relation* $F_\nu \propto \nu^{-0.584}$*. The Chandra observations are now directly comparable to the VLA data, allowing for a comprehensive analysis of the emission at different frequencies.*

4. MEASURES OF THE AMOUNT OF RADIATION

4.1 Radiation Physics definitions

1. **Luminosity (L)** or power is the rate at which energy is emitted. Its SI units are J s^{-1} or watts (1 W = 1 J s^{-1}) and erg s^{-1} in cgs. One calculates a source's luminosity or power by dividing the amount of energy emitted by the length of time over which the energy was emitted. This yields the rate of emission.

2. The radiation power that we detect depends on the size of our telescope—the larger its cross-sectional area, the more radiation will be detected—so we again wish to normalize our measurement, this time, by dividing by the area of the telescope. This gives the **measure of flux** (F), that is, the amount of light energy per unit time per unit area. The units of flux are J s^{-1} m^{-2} or W m^{-2} (SI) and ergs s^{-1} cm^{-2} (cgs).

3. **Flux density (F_ν or F_λ)** is the flux per unit frequency in the observed spectral range, and it equals the detected flux divided by the width in frequency of the observation. Therefore,

   $$F_\nu = \frac{F}{\Delta\nu}$$

   where: F_ν is the flux density, F is the detected flux, $\Delta\nu$ is the bandwidth or the range in frequency of the detected electromagnetic waves.

4. **Intensity (I_ν or I_λ)**, also known as specific intensity, surface brightness, or simply brightness, is the flux density per unit solid angle.

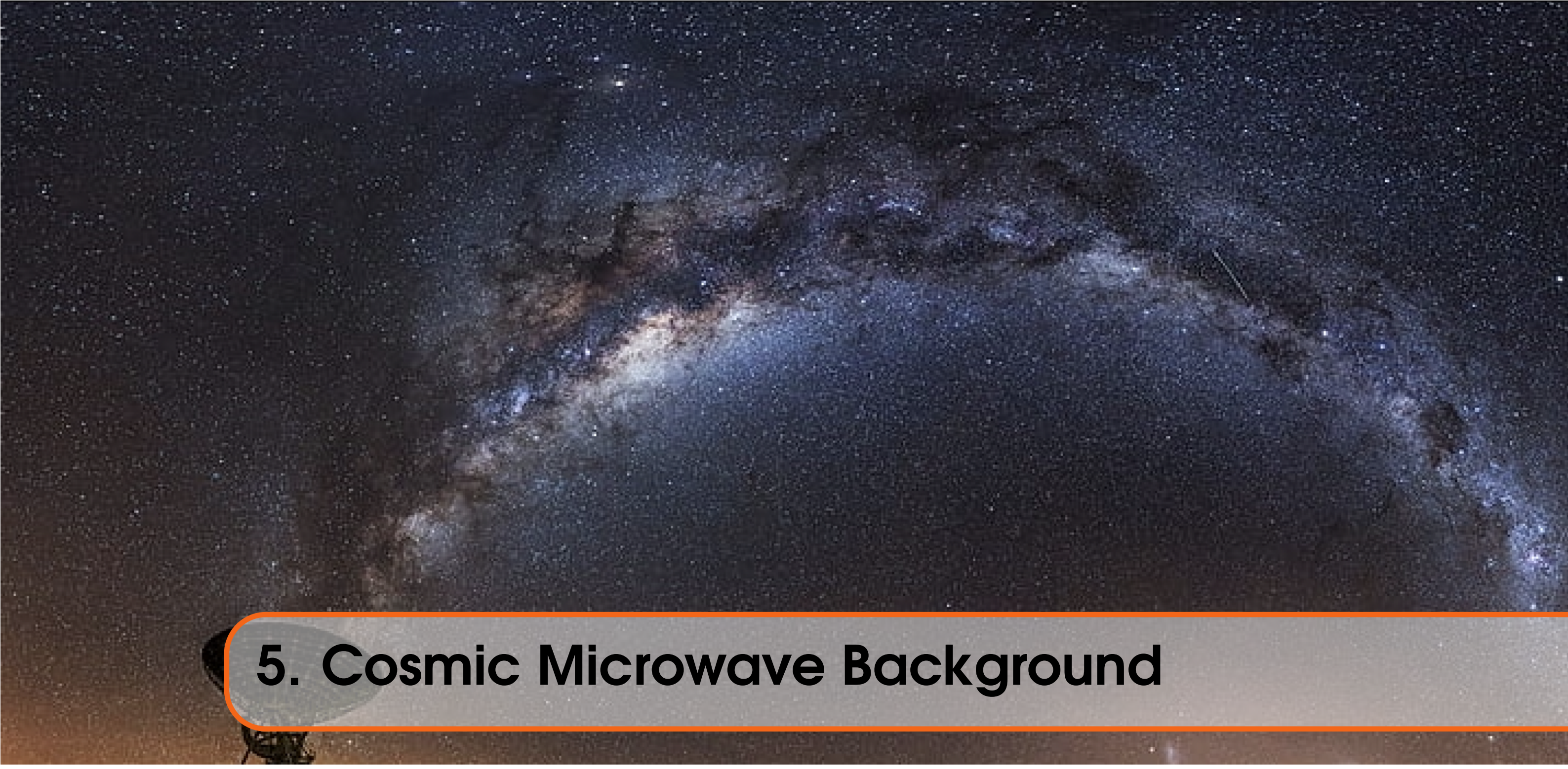

5. Cosmic Microwave Background

The Cosmic Microwave Background (CMB) (10) , originating approximately 400,000 years after the Universe's inception, provides a snapshot of the early cosmos. While this period may seem brief in human terms, it represents only a tiny fraction of the Universe's immense 13.7-billion-year history. Prior to this epoch, the Universe was incredibly hot and dense, rendering it opaque to all forms of radiation. Even basic atoms couldn't exist, as they would swiftly disintegrate into their constituent protons and electrons due to the intense radiation. During this phase, the Universe consisted of a plasma, akin to the ionized gas found on the Sun's surface.

Since the Big Bang, the Universe has been gradually cooling and expanding. After approximately 400,000 years, it cooled enough (although still at around 3000 degrees Celsius) for the simplest atoms to form, causing it to become transparent. The light emitted during this period has been traveling through space ever since, and we can detect it all around us, both on Earth and in space. This afterglow of the Big Bang is known as the Cosmic Microwave Background (CMB).

The expansion of the Universe has stretched out the CMB radiation by around 1000 times, which makes it look much cooler. So instead of seeing the afterglow at 3000 degrees, we see it at just 3o above absolute zero, or 3 Kelvin (-270o C). Just as a burning coal (around 1500 K) glows red, and a hot bright star (around 6000 K) glows yellow or blue, the CMB glow with a characteristic colour associated with it's temperature. However, because it is so cold, the light which was emitted by the glowing Universe now has a much longer wavelength than we can see with our eyes. The CMB is brightest at a wavelength of around 2 mm, which is around 4000 times longer than the wavelength of the visible light we see with our eyes.

5.1 Planck's Function

The Planck function provides a mathematical description of the spectrum of the light emitted by blackbodies. In terms of the emitted flux per unit frequency interval per unit steradian, the Planck function is given by:

$$B_T(\nu) = \frac{2h}{c^2} \cdot \frac{\nu^3}{e^{\frac{h\nu}{kT}} - 1}$$

where: $h = 6.626 \times 10^{-34}$
J s $= 6.626 \times 10^{-27}$
erg s is Planck's constant, $k = 1.38 \times 10^{-23}$ J K^{-1} $= 1.38 \times 10^{-16}$ ergs K^{-1} is Boltzmann's constant, c is the speed of light,
ν is the frequency of the observation,
T is the temperature of the radiating body in Kelvins.

5.2 Curve Fitting

We will use far infrared data adapted from the COBE (7)satellite to fit a blackbody curve to the CMB. We read the file into python and make a plot showing the brightness as a function of frequency. Knowing that it is a blackbody spectrum, we fit the blackbody function to the data with temperature as the free parameter. We obtain the following result:

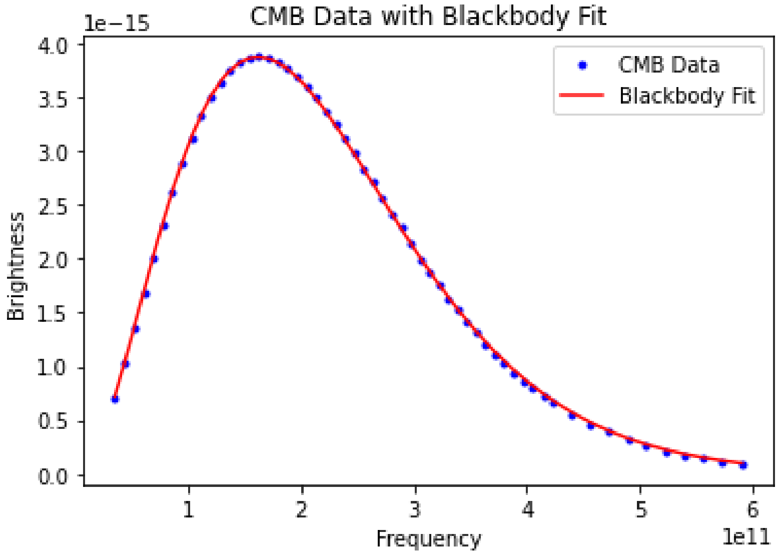

Figure 5.1: **Cosmic Microwave Background (CMB) Blackbody Fit:** *The plot displays the CMB data points (in blue) along with the blackbody fit (in red) obtained using the blackbody function. The blackbody fit provides a good fit to the CMB data, allowing us to determine the fitted temperature and scale. The* $temperature_fit$ *represents the fitted temperature of the CMB, and* $scale_fit$ *corresponds to the scale factor applied to the blackbody function to match the data.*

Using the blackbody function, we get the optimized CMB temperature to be **2.75 Kelvin**

6. Hydrogen 21 cm Line

6.1 Introduction

21 centimeter radiation arises as a consequence whenever new stars are produced. Every time that a star-forming event occurs, the more massive newborn stars produce large amounts of ultraviolet radiation: radiation that's energetic enough to ionize hydrogen atoms. All of a sudden, space that was once filled with neutral hydrogen atoms is now filled with free protons and free electrons.

But those electrons are going to eventually be captured, once again, by those protons, and when there's no longer enough ultraviolet radiation to ionize them over and over again, the electrons will once again sink down to the ground state, where they'll have a 50/50 chance of being aligned or anti-aligned with the spin of the atomic nucleus.

Again, that same radiation — of 21 centimeters in wavelength — gets produced, and every time we measure that 21 centimeter wavelength localized in a specific region of space, even if it gets redshifted by the expansion of the Universe, what we're seeing is evidence of recent star-formation. Wherever star-formation occurs, hydrogen gets ionized, and whenever those atoms become neutral and de-excite again, this specific-wavelength radiation persists for tens of millions of years.

6.2 Galaxy Rotation Curve

To obtain the galaxy rotation curve, we will use synthetic spectra available for different spectrums of different distance intervals within that is a Hydrogen 21 cm line at a Doppler velocity. We fit for the Doppler velocity of the 21 cm line for each distance. To do so, we fit a gaussian to the spectral line and determine the central frequency. We Use the displacement from the expected value to find the velocity. Once all lines are done, plot the velocities as a function of distance from the centre of our galaxy.

The Gaussian fit to the spectral line for all the spectrums come out to be:

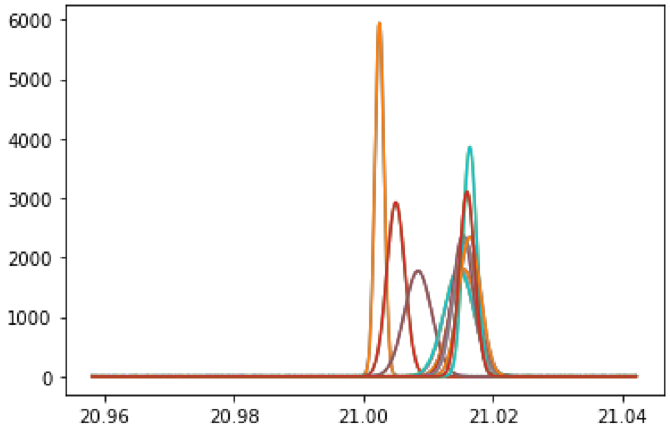

Figure 6.1: **Gaussian fit**: *The plot shows the Gaussian fit overlaid on the original spectrum data points (in b. The Gaussian fit is obtained using the* $curve_fit$ *function, which calculates the best-fit parameters for the amplitude, mean, and standard deviation. This fit allows us to model and analyze the spectral line shape accurately.*

The Galaxy Rotation curve after finding all the corresponding velocities come out to be:

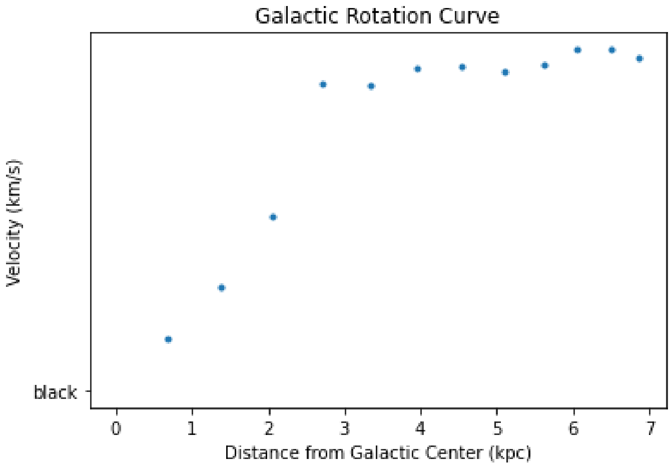

Figure 6.2: **Galactic Rotation Curve:** *The plot shows the rotation velocities of galaxies as a function of their distance from the Galactic Center (kpc). The observed velocities deviate from the expected Newtonian curve, indicating the presence of unseen mass, possibly dark matter, influencing galactic dynamics.*

7. Radio Telescopes

7.1 RADIO TELESCOPE REFLECTORS, ANTENNAS, AND FEEDS

7.1.1 Primary Reflectors

Most radio telescopes employ parabolic reflectors, similar to the primary components of telescopes used in other wavelength regimes such as infrared, visible, and ultraviolet. The parabolic shape of the dish ensures that all waves arriving from the direction perpendicular to the entrance plane converge at a single focal point, known as the telescope's focus. As the electromagnetic waves emitted by celestial objects travel over vast distances to reach our telescope, they can be accurately approximated as plane waves, allowing them to enter the telescope in parallel paths.

7.1.2 Beam Pattern

The beam pattern of a radio telescope characterizes its ability to detect radio signals from different angles in the sky. It is similar to the point-spread function used in optical astronomy, representing the sensitivity distribution of the telescope. Whether the antenna is receiving or transmitting, the sensitivity pattern remains the same, thanks to the reciprocity theorem. Ideally, each feed in the telescope would collect signals from only one specific direction, ensuring that when the telescope is pointed towards a particular spot, the detected power corresponds exclusively to the radiation coming from that location. However, achieving this ideal scenario is hindered by the phenomenon of diffraction, which affects various types of waves passing through an aperture or opening, causing partial blockage of the wavefront.

7.1.3 Feeds and Primary Reflector Illumination

At the focal point of a radio telescope, antennas are employed to transform the electromagnetic waves from free space into confined waves within transmission lines. This enables the transmission of these waves to the receivers. Each feed in the telescope is connected to a single receiver, which generates a single measurement of detected power. Typically, horn antennas with either rectangular or circular cross-sections are utilized as the feeds. These horn antennas are often flared, allowing radiation to enter through the larger end and gradually tapering down to the appropriate size (in proportion to the observed wavelength) for a waveguide transmission line.

The flared end of the horn antenna possesses a size that is at least as large as the wavelength of the observed light, although the exact size depends on the telescope's optical design. For telescopes operating at longer wavelengths, such as the Haystack Small Radio Telescope (SRT), the minimum size of the feed horn opening can be quite large, limiting the number of feeds that can be accommodated in the focal plane. Consequently, only one feed can fit in the focal plane of the SRT, allowing power measurements to be taken from only one position during each telescope pointing. Conversely, larger telescopes operating at millimeter and submillimeter wavelengths can often employ an array of feeds, enabling multiple positions to be observed simultaneously in a single pointing.

7.1.4 Surface errors

The primary reflector of a radio telescope is never a perfect parabola due to manufacturing imperfections that limit its surface accuracy. To characterize an imperfect reflector, we measure the root mean square (rms) deviations, dz, of the real surface from an ideal parabola along the optical axis. These deviations cause variations in the path length to the focus for different parts of the reflector, leading to phase differences and less than full constructive interference. As a result, the power collected by the telescope is reduced. Since the light is reflected off the surface, the total path difference is twice the deviation (2dz), resulting in rms phase errors of $\frac{4\pi dz}{\lambda}$.

7.2 Noise, Noise Temperature and Antenna Temperature

(6)
The components in the receiver, especially the amplifiers, generate their own electrical signals that propagate through the receiver and are unrelated to the signal from the astronomical source. The power measured coming out of the detector includes these extra signals, which interfere with our ability to detect and measure the power of the radiation from the astronomical source. These extra signals are undesirable but cannot be avoided. We call this unwanted signal noise. It is necessary to be aware of the noise and know how to account for it. It is also desirable for the receiver to be designed to minimize the noise as much as possible.

Characterizing noise signals generated in electrical circuits has always been of great interest in electronics. Radio astronomers also describe the power traveling in the transmission lines and receiver in terms of an equivalent temperature given by

$$T_{\text{equiv}} = \frac{\Delta\nu}{kP}$$

where: - k is Boltzmann's constant, - $\Delta\nu$ is the bandwidth of the radiation with power P.
Some of the detected power is due to the astronomical source, which was converted by the antenna to electronic power in the transmission line. We call the equivalent temperature of the power that the antenna delivers to the transmission line the antenna temperature, T_A. However, the far majority of the detected power is due to noise from the receiver components. We describe the total noise power by the noise temperature, T_N, and each component in the receiver is characterized by its own noise temperature. We need to discuss how the final power measured in the output of the receiver relates to the antenna temperature and the noise temperature of each of the components. It's important to note that both the source signals and the noise are affected by the amplification and losses that occur along the path through the receiver. Thus, the equivalent temperature of the final power output is not simply the sum of the equivalent temperatures of all the sources in the path.

Now, let's focus on the signal from the astronomical source and see how its power is affected by the processes in the receiver. At each stage, the source signal is either amplified (when passing through an amplifier) or reduced by a loss (such as in a transmission line or in the mixer). We can use the gain, G, defined by Equation 3.3, for each step. For example, if we assign a gain of G_1 to the first element, which is the RF amplifier, then the power in the source signal after this stage is

$$P = G_1 kT\Delta\nu A$$

By the time the signal enters the detector, the power due to the radiation entering the antenna has been amplified by a net gain, G, and so

$$P = GkT\Delta\nu A$$

The antenna temperature describes the power in the input radiation before any amplification. Even though the amount of power increases when the signal is passed through an amplifier, the radiation is still described by the same equivalent temperature. Therefore, regardless of the amount of amplification in the system, the input radiation power will still be described by the same antenna temperature. Now, since we need to compare the noise power with the power from the astronomical source, we must describe both powers in the same way. In particular, an amplifier's noise temperature is defined by the equivalent temperature of the noise power as if it was introduced at the input to the amplifier, and hence it is amplified along with the astronomical signal. Imagine, for example, that the receiver contained only an amplifier of gain G_1 and noise temperature T_{N1}. Then, the power output would be

$$P = \frac{G}{1+\frac{G_1}{G}} kT\Delta\nu A + T_1$$

So, the antenna temperature and noise temperature, with this convention of defining T_{N1}, are directly comparable.

II

Part Two

8 Radio Astronomy Observing Basics . . . 31
8.1 Two element interferometer
8.2 Observation of a single point source
8.3 Visibility equation for a general extended source

9 Common Astronomy Software Applications 35
9.1 CASA
9.2 TW Hydra
9.3 Supernova Remnant 3C 391

10 Markov-Chain Monte Carlo (MCMC) . 47

11 Fast Radio Bursts 53

8. Radio Astronomy Observing Basics

8.1 Two element interferometer

A basic two-element interferometer is a simple configuration used in radio astronomy to study celestial sources. It consists of just two radio antennas or dishes separated by a fixed distance, forming the two elements of the interferometer. This configuration is also known as a baseline, where the baseline length is the distance between the two antennas.

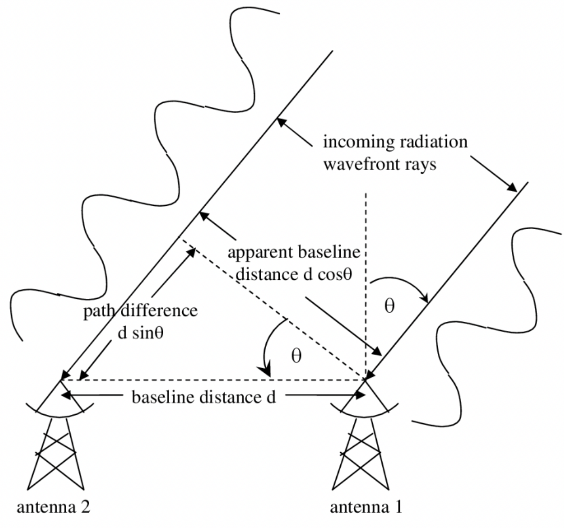
incoming radiation
wavefront rays
apparent baseline
distance d cosθ
path difference
d sinθ
θ
θ
baseline distance d
antenna 2
antenna 1

Figure 8.1: Two element interferometer

8.2 Observation of a single point source

Flux calibration is an essential process in radio astronomy and interferometry to convert the recorded signals from radio telescopes into physical units of flux density (usually expressed in units like Jansky, mJy, or Jy/beam). This calibration is necessary because the data obtained from radio telescopes are typically recorded in arbitrary units called counts or analog-to-digital units (ADU) that do not directly represent physical quantities. We observe a bright source of *known* flux density.

The primary goal of flux calibration is to establish a relationship between the recorded signal amplitudes (counts or ADU) and the actual flux density of the astronomical sources being observed. To achieve this, radio astronomers observe known astronomical sources with accurately measured flux densities. These sources are often called "flux calibrators" or "flux calibrations standards."

One common type of flux calibrator used in radio astronomy is a "point source," which is an astronomical object that appears as a single point-like source in the radio telescope's field of view. Point sources are ideal for flux calibration because their emission is concentrated at a single location, simplifying the calibration process. Examples of point sources often used for calibration include compact radio galaxies, quasars, and certain radio-bright stars. The amplitude of fringes equals the flux density of the point source.

$$R = F_\nu cos(2\pi \frac{bsin(\omega_e t)}{\lambda})$$

Here, ω_e is the angular velocity of the Earth, b is the baseline length i.e length between the two antennas.

The process of **phase calibration** involves observing a bright and known position source, often referred to as a "phase calibrator" or "calibration source," multiple times during the observing session. This calibration source should be close in the sky to the target source of interest, ideally within a few degrees.

By repeatedly observing the phase calibrator and applying the derived phase offsets to the target source data, radio astronomers can significantly improve the quality of their observations. Phase calibration is crucial for obtaining high-resolution and high-fidelity images, especially for extended or complex astronomical sources.

$$R = F_\nu cos(2\pi \frac{bsin(\omega_e t)}{\lambda} + \Delta\phi) = F_\nu cos(2\pi \frac{bsin(\omega_e t)}{\lambda} + 2\pi \frac{b\Delta\theta}{\lambda})$$

8.3 Visibility equation for a general extended source

The visibility equation is a fundamental concept in radio astronomy and interferometry. It describes the relationship between the measured visibility, which is the complex amplitude of the interference pattern observed by an interferometer, and the brightness distribution of a celestial source in the sky.

In radio interferometry, multiple antennas are used to observe the same astronomical source simultaneously. Each antenna collects radio waves from the source, and the signals are combined to create an interference pattern. The visibility equation relates this interference pattern to the brightness distribution of the source.

The visibility equation is a fundamental concept in radio astronomy and interferometry. It describes the relationship between the measured visibility, which is the complex amplitude of the interference pattern observed by an interferometer, and the brightness distribution of a celestial source in the sky.

In radio interferometry, multiple antennas are used to observe the same astronomical source simultaneously. Each antenna collects radio waves from the source, and the signals are combined to create an interference pattern. The visibility equation relates this interference pattern to the brightness distribution of the source.

The visibility equation is given by:

$$V(u,v) = \int\int I(l,m) \cdot e^{-2\pi i(ul+vm)}\, dl\, dm$$

Where: $V(u,v)$ is the measured visibility at a particular baseline with spatial frequency components u and v. $I(l,m)$ is the brightness distribution of the celestial source as a function of the direction cosines l and m on the sky. e is the Euler's number (approximately equal to 2.71828). i is the imaginary unit ($i^2 = -1$). u and v are the spatial frequencies of the baseline, which are determined by the separation between the two antennas and the observed wavelength.
The visibility equation is essentially a 2D Fourier transform, where the brightness distribution of the source on the sky $I(l,m)$ is transformed into the visibility pattern in the $u-v$ plane $V(u,v)$. This equation allows radio astronomers to extract information about the source's brightness distribution and its spatial structure.

By observing a range of different baselines (u and v values), radio interferometers sample different spatial scales of the observed source. Combining data from multiple baselines and using advanced data processing techniques, astronomers can reconstruct high-resolution images of celestial objects and study their physical properties in detail.

The visibility equation is a key component of radio interferometry, enabling astronomers to obtain high-angular resolution and sensitivity, which is essential for studying a wide range of astrophysical phenomena, including stars, galaxies, black holes, and cosmic masers.

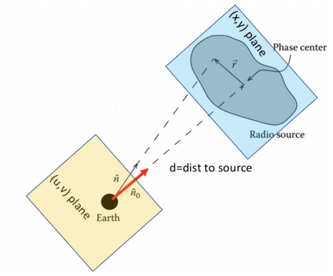

Figure 8.2: Projection Of U-V Plane Coordinates

9. Common Astronomy Software Applications

9.1 CASA

CASA (Common Astronomy Software Applications) is a widely used software package for data reduction, calibration, and imaging in radio astronomy.
CASA is primarily designed to run on Linux and macOS operating systems. If you are using one of these systems, you can easily install CASA directly on your machine following the installation instructions provided by the CASA team.
However, if you are using a different operating system, like Windows, setting up a Linux Virtual Machine (VM) is a practical solution. A Linux VM allows you to run a Linux-based operating system within your current OS environment. You can install CASA on the Linux VM and perform radio astronomy data processing within that virtual environment.

9.2 TW Hydra

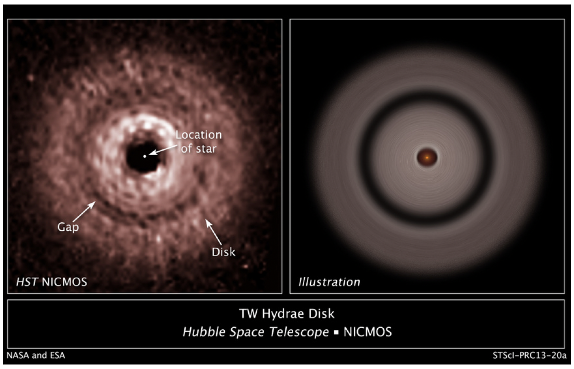
Location of star
Gap
Disk
HST NICMOS
Illustration
TW Hydrae Disk
Hubble Space Telescope ▪ NICMOS
NASA and ESA
STScI-PRC13-20a

Figure 9.1: TW Hydrae Protoplanetary Disk: Gap in a protoplanetary disk of dust and gas whirling around the nearby red dwarf star TW Hydrae.

This image (11) captures a gap in the protoplanetary disk of dust and gas surrounding the nearby red dwarf star, TW Hydrae. The presence of this gap suggests the influence of an unseen, growing planet that is gravitationally collecting material and creating a lane in the disk, similar to a snow plow. The Hubble Space Telescope image on the left shows the gap, situated approximately 7.5 billion miles away from the central star. If this hypothetical planet were in our solar system, it would be about twice as far from the Sun as Pluto. The image, taken in near-infrared light by the Near Infrared Camera and Multi-Object Spectrometer (NICMOS), was achieved by using a masking device to block the star's bright light, revealing the structure of the disk. The observations indicate that the gap, which spans 1.9 billion miles, is not completely cleared out. TW Hydrae is located 176 light-years away in the Hydra constellation.

Now, our task is to image TW Hydra using CASA Software. The data which will be used for this task was obtained from the interferometer Atacama Large Millimeter Array (ALMA) (9).

We use this site to learn how to image. (4)

9.2.1 Getting information of the object

To get the information relating the target, we use :

```
    # In CASA
    listobs(vis='sis14_twhya_calibrated_flagged.ms')
```

On running this, we see that the field associated with TW Hydra is 5.

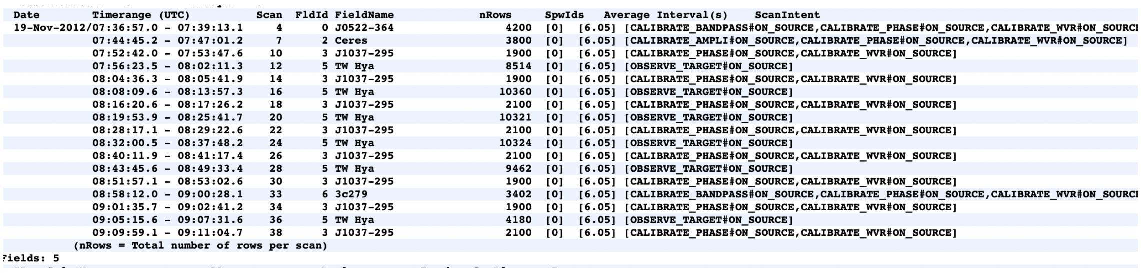

```
 Date          Timerange (UTC)          Scan  FldId FieldName              nRows     SpwIds   Average Interval(s)    ScanIntent
 19-Nov-2012/07:36:57.0 - 07:39:13.1       4      0 J0522-364               4200  [0]  [6.05] [CALIBRATE_BANDPASS#ON_SOURCE,CALIBRATE_PHASE#ON_SOURCE,CALIBRATE_WVR#ON_SOURC
             07:44:45.2 - 07:47:01.2       7      2 Ceres                   3800  [0]  [6.05] [CALIBRATE_AMPLI#ON_SOURCE,CALIBRATE_PHASE#ON_SOURCE,CALIBRATE_WVR#ON_SOURCE]
             07:52:42.0 - 07:53:47.6      10      3 J1037-295               1900  [0]  [6.05] [CALIBRATE_PHASE#ON_SOURCE,CALIBRATE_WVR#ON_SOURCE]
             07:56:23.5 - 08:02:11.3      12      5 TW Hya                  8514  [0]  [6.05] [OBSERVE_TARGET#ON_SOURCE]
             08:04:36.3 - 08:05:41.9      14      3 J1037-295               1900  [0]  [6.05] [CALIBRATE_PHASE#ON_SOURCE,CALIBRATE_WVR#ON_SOURCE]
             08:08:09.6 - 08:13:57.3      16      5 TW Hya                 10360  [0]  [6.05] [OBSERVE_TARGET#ON_SOURCE]
             08:16:20.6 - 08:17:26.2      18      3 J1037-295               2100  [0]  [6.05] [CALIBRATE_PHASE#ON_SOURCE,CALIBRATE_WVR#ON_SOURCE]
             08:19:53.9 - 08:25:41.7      20      5 TW Hya                 10321  [0]  [6.05] [OBSERVE_TARGET#ON_SOURCE]
             08:28:17.1 - 08:29:22.6      22      3 J1037-295               2100  [0]  [6.05] [CALIBRATE_PHASE#ON_SOURCE,CALIBRATE_WVR#ON_SOURCE]
             08:32:00.5 - 08:37:48.2      24      5 TW Hya                 10324  [0]  [6.05] [OBSERVE_TARGET#ON_SOURCE]
             08:40:11.9 - 08:41:17.4      26      3 J1037-295               2100  [0]  [6.05] [CALIBRATE_PHASE#ON_SOURCE,CALIBRATE_WVR#ON_SOURCE]
             08:43:45.6 - 08:49:33.4      28      5 TW Hya                  9462  [0]  [6.05] [OBSERVE_TARGET#ON_SOURCE]
             08:51:57.1 - 08:53:02.6      30      3 J1037-295               1900  [0]  [6.05] [CALIBRATE_PHASE#ON_SOURCE,CALIBRATE_WVR#ON_SOURCE]
             08:58:12.0 - 09:00:28.1      33      6 3c279                   3402  [0]  [6.05] [CALIBRATE_BANDPASS#ON_SOURCE,CALIBRATE_PHASE#ON_SOURCE,CALIBRATE_WVR#ON_SOURC
             09:01:35.7 - 09:02:41.2      34      3 J1037-295               1900  [0]  [6.05] [CALIBRATE_PHASE#ON_SOURCE,CALIBRATE_WVR#ON_SOURCE]
             09:05:15.6 - 09:07:31.6      36      5 TW Hya                  4180  [0]  [6.05] [OBSERVE_TARGET#ON_SOURCE]
             09:09:59.1 - 09:11:04.7      38      3 J1037-295               2100  [0]  [6.05] [CALIBRATE_PHASE#ON_SOURCE,CALIBRATE_WVR#ON_SOURCE]
           (nRows = Total number of rows per scan)
Fields: 5
```

Figure 9.2: Part of the output of listobs

9.2.2 Interactive Cleaning of the image

First job is to clean the image. To achieve this, we use the command *tclean* in CASA.

```
# In CASA
os.system('rm -rf twhya_cont.*')

tclean(vis='twhya_smoothed.ms',
       imagename='twhya_cont',
       field='0',
       spw='',
       specmode='mfs',
       gridder='standard',
       deconvolver='hogbom',
       imsize=[250,250],
       cell=['0.08arcsec'],
       weighting='briggs',
       robust=0.5,
       threshold='0mJy',
       niter=5000,
       interactive=True)
```

Listing 9.1: tclean parameters

Task tclean is powerful with many inputs and a certain amount of experimentation likely is required.

After running this in CASA, we get a continuum image of TW Hydra, which looks like this:

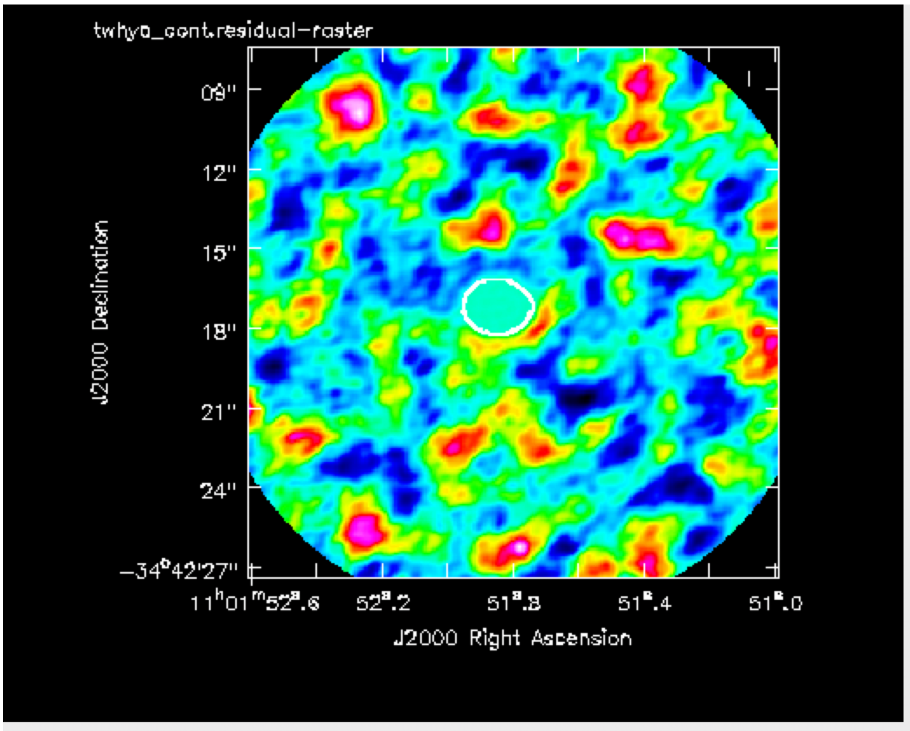

Figure 9.3: Image after 300 iterations of interactive cleaning

We will begin by creating a clean mask around the visible emission of the TW Hydra disk using the mask tools. This mask will help specify the region of interest for tclean to focus on during the cleaning process. Then, we will run tclean in interactive mode, giving us the control to decide when to stop the cleaning process. Throughout the cleaning, we will carefully observe the progress and decide when the emission from the TW Hydra disk is reduced to an acceptable level, comparable to the residuals around it. Once we are satisfied with the cleaning results, we will simply hit the red X to stop tclean, indicating that the cleaning process should come to an end. This interactive cleaning approach allows us to have full control over the cleaning process, ensuring that we achieve the desired level of cleaning for the visible emission.

Once this interactive cleaning process is done, we view the new image. We do this by running the following command:

```
#In CASA
imview("twhya_cont.image")
```

TW Hydra is very bright and WE can see that it is extended relative to the size of the beam, which is represented by an oval at the bottom of the panel.

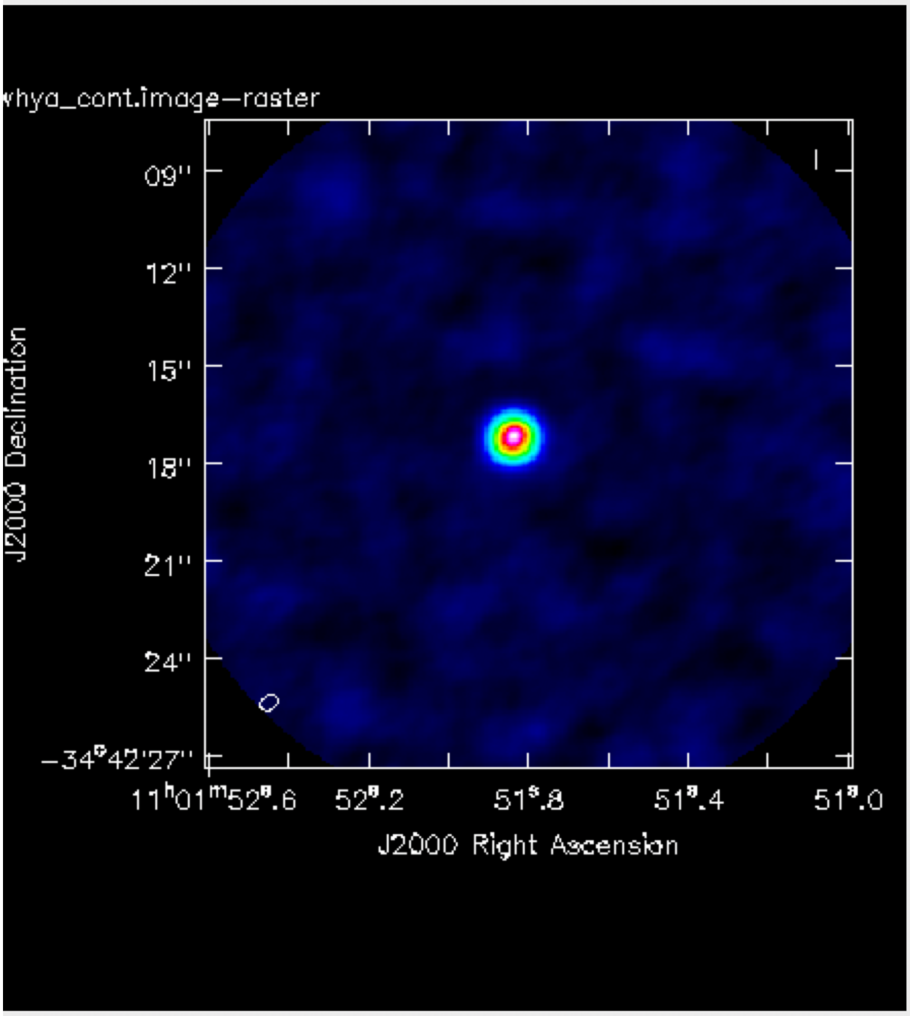
hya_cont.image−raster
J2000 Declination
09''
12''
15''
18''
21''
24''
−34°42'27''
11h01m52s.6
52s.2
51s.8
51s.4
51s.0
J2000 Right Ascension

Figure 9.4: Continuum image of TW Hydra

9.2.3 Non-interactive clean

We have primarily followed an **interactive** process with tclean, giving us the flexibility to make real-time decisions based on the cleaning progress. However, tclean can also be utilized in a non-interactive mode, where we specify three key parameters. First, we set a threshold value, and tclean automatically stops once the maximum residual in the tclean region falls below this threshold, ensuring the cleaning process halts at an acceptable level of residuals. Next, we define a mask that guides tclean to focus solely on specific regions of interest, streamlining the cleaning process and reducing unnecessary computations. Finally, although not obligatory, we can set a maximum number of iterations as a precautionary measure. By choosing a high value, we ensure that if tclean reaches this limit, it alerts us to potential issues in the data or cleaning strategy. Employing tclean without interactive guidance provides us with an automated data-cleaning approach, offering enhanced efficiency in handling vast datasets and complex radio astronomy sources.

To determine a clean mask, we examined the image generated earlier, where all the obvious emission is confined within a box bounded by pixel numbers ranging from approximately (100,100) to (150,150). We will use this box as the mask by specifying the "mask" parameter in the call to tclean. Alternatively, we could have supplied a file containing the mask, created from a previous interactive version of tclean.

Next, we aim to set a stopping threshold for tclean. By observing the previous image using imview, we identified a region well away from the source to estimate the noise. To avoid introducing false sources into the deconvolved image, it is generally recommended to set a clean threshold that is several times the rms noise level. This ensures that tclean does not mistake random noise spikes as sources and avoid deconvolving them from the image. For our purposes, we will set niter=10000, an ample number of iterations, with the expectation that tclean will terminate before reaching this limit. This large value acts as a safeguard, preventing tclean from running indefinitely.

By configuring tclean with the clean mask, appropriate threshold, and maximum iterations, we can conduct a robust and efficient data-cleaning process, avoiding potential pitfalls associated with false detections and ensuring the convergence of the cleaning algorithm.

We perform non-interactive clean in the following manner:

```
#In CASA
os.system('rm -rf twhya_cont_auto.*')

tclean(vis='twhya_smoothed.ms',
       imagename='twhya_cont_auto',
       field='0',
       spw='',
       specmode='mfs',
       gridder='standard',
       deconvolver='hogbom',
       imsize=[250,250],
       cell=['0.08arcsec'],
       mask='box [ [ 100pix , 100pix] , [150pix, 150pix ] ]',
       weighting='briggs',
       robust=0.5,
       threshold='15mJy',
       niter=10000,
       interactive=False)
```

After doing this, we can view the image:

```
    imview('twhya_cont_auto.image')
```

The noninteractive mode in tclean can save a considerable amount of time and has the advantage of being highly reproducible. However, there is also a "hybrid" mode available, which involves initiating the tclean process with "interactive=True" and then clicking the blue arrow button in the top right corner. This hybrid mode instructs tclean to proceed until it reaches the maximum number of iterations or the specified threshold. The advantage of this mode is that you can manually draw the mask used for tclean, offering additional flexibility in the cleaning process. Moreover, you have the option to manually set both the threshold and the maximum number of iterations in the viewer GUI, allowing for more tailored control.

It is important to note that, particularly for images with uncertain calibration or bright sources, it is recommended to clean interactively at least during the initial cleaning phase. Interactive cleaning enables real-time adjustments and provides better control over the cleaning process in such situations. In cases where an image may be "dynamic range limited," meaning that the image quality is limited by the accuracy of calibration and deconvolution, it can be challenging to predict the correct threshold.

As the cleaning cycles proceed, the residuals in the image should gradually decrease. To monitor this, you can check the tclean output in the logger. If, at any point, the residuals start to increase, it may indicate the need to adjust the stopping threshold to ensure effective cleaning and achieve a cleaner final image.

The final image looks like the following:

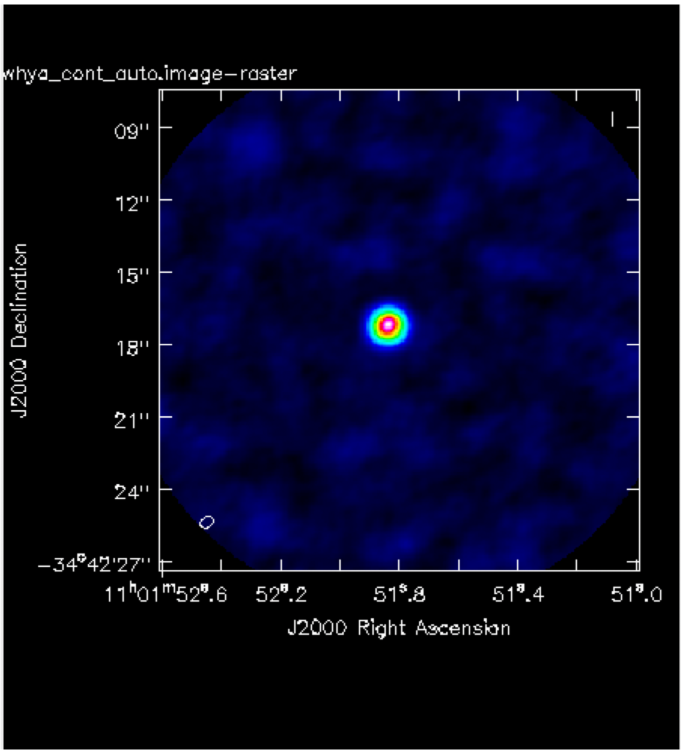

Figure 9.5: Non interactive cleaned image, until the threshold is reached.

9.2.4 Primary Beam Correction

An important subtlety of tclean (and clean) is that the default image produced by tclean is not corrected for the primary beam (the field of view) of the individual dishes in the array. The primary beam response is typically a Gaussian with a value of 1 at the center of the field. To obtain an astronomically correct image of the sky, the output of tclean needs to be divided by this primary beam (or, in the case of mosaics, the combination of primary beam patterns used to make the mosaic).

For tclean, there are two ways to perform this correction. First, you can set the parameter "pbcor=True" when running tclean. This will produce an additional image with the extension ".image.pbcor," which represents the cleaned image corrected for the primary beam.

Alternatively, CASA stores the primary beam information needed for the correction in the file with the ".pb" extension. To apply the primary beam correction, you can use the CASA task "impbcor," which combines the ".pb" image with the output image from tclean, resulting in a primary-beam corrected image.

Before applying the primary beam correction, it is important to ensure that any pre-existing primary beam corrected image is removed, if present. This ensures the accuracy and consistency of the final primary-beam corrected output image. To do so, we run the following command:

```
    # In CASA
    os.system('rm -rf twhya_cont.pbcor.image')
```

Now we correct the image:

```
    # In CASA
impbcor(imagename='twhya_cont.image',
        pbimage='twhya_cont.pb',
        outfile='twhya_cont.pbcor.image')
```

After this we inspect the new image:

```
    # In CASA
    imview('twhya_cont.pbcor.image')
```

The corrected primary beam image that we get is as follows:

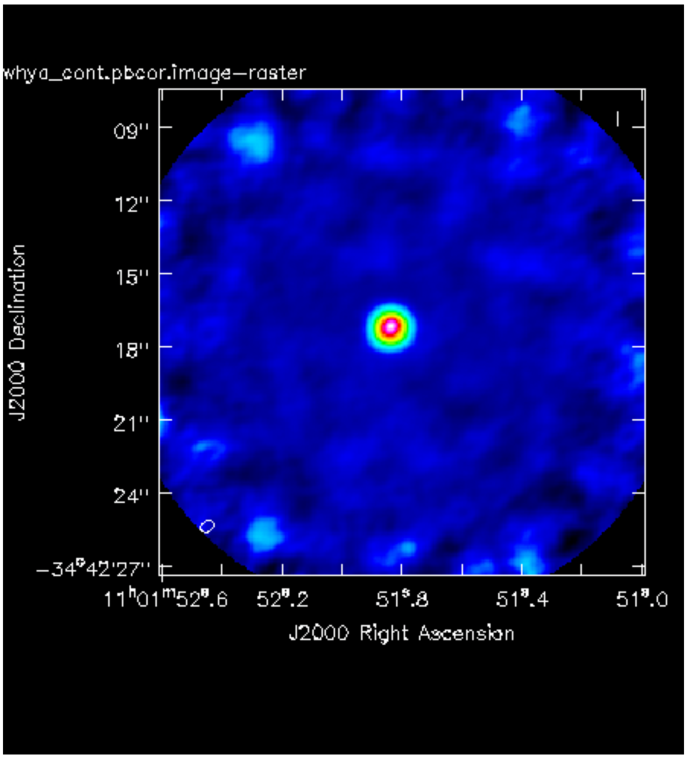
whya_cont.pbcor.image–raster
09''
12''
15''
18''
21''
24''
−34°42'27''
J2000 Declination
11h01m52s.6
52s.2
51s.8
51s.4
51s.0
J2000 Right Ascension

Figure 9.6: Primary Beam Corrected Image

9.2.5 Statistics

There are different ways to see the statistics of the source. One way is to box the region and see the statistics in the image viewer. Another way is to directly use the imstat command to get the required statistics.

I have boxed the source region and looked at the statistics as given below:

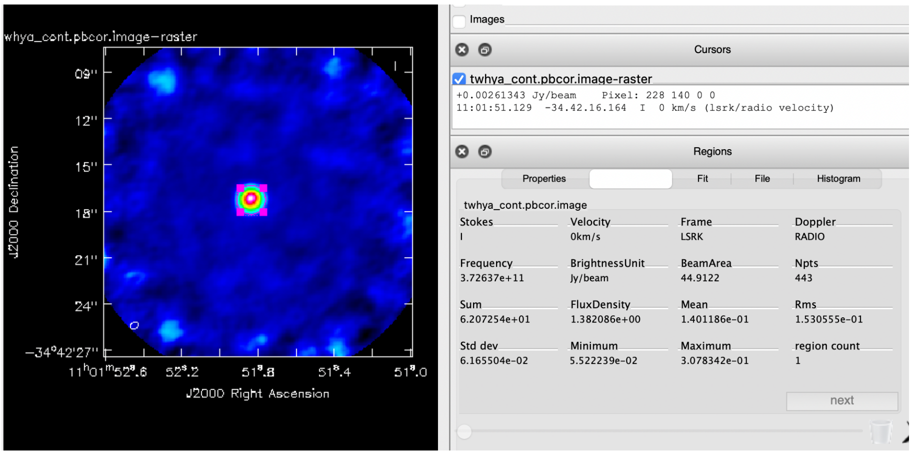
whya_cont.pbcor.image–raster
09''
12''
15''
18''
21''
24''
−34°42'27''
J2000 Declination
11h01m52s.6
52s.2
51s.8
51s.4
51s.0
J2000 Right Ascension
☐ Images
Cursors
Regions
Properties
Fit
File
Histogram
next

☑ twhya_cont.pbcor.image-raster

```
+0.00261343 Jy/beam    Pixel: 228 140 0 0
11:01:51.129  -34.42.16.164  I  0 km/s (lsrk/radio velocity)
```

twhya_cont.pbcor.image

Stokes	Velocity	Frame	Doppler
I	0km/s	LSRK	RADIO
Frequency	**BrightnessUnit**	**BeamArea**	**Npts**
3.72637e+11	Jy/beam	44.9122	443
Sum	**FluxDensity**	**Mean**	**Rms**
6.207254e+01	1.382086e+00	1.401186e-01	1.530555e-01
Std dev	**Minimum**	**Maximum**	**region count**
6.165504e-02	5.522239e-02	3.078342e-01	1

Figure 9.7: Statistics by boxing the region of the source

9.3 Supernova Remnant 3C 391

(3)

9.3.1 Imaging

In radio astronomy, the visibility data and the sky brightness distribution (image) are related as Fourier transform pairs. The coordinates involved are as follows:

- The u and v coordinates represent the baselines measured in units of the observing wavelength.
- The l and m coordinates represent the direction cosines on the sky.

For simplicity, the sky coordinates are often written in terms of direction cosines, but in most VLA (and ALMA) observations, they can be directly related to the right ascension (α) and declination (δ). It is important to note that this relationship is valid only if the w coordinate of the baselines can be neglected. This assumption is generally true at higher frequencies and smaller VLA configurations, such as the 4.6 GHz D-configuration observations. However, at lower frequencies and larger configurations, such as 0.33 GHz A-configuration observations, the w coordinate cannot be neglected. Additionally, this expression neglects other factors, such as the shape of the primary beam.

The relationship between the visibility ($V(u,v)$) and the sky brightness distribution ($I(l,m)$) can be expressed as:

$$V(u,v) = \int\int I(l,m) \cdot e^{-2\pi i(ul+vm)}\, dl\, dm$$

9.3.2 Multi-scale Mosaic Clean

We will run the cleaning task interactively so that we can set and modify the mask:

```
    # In CASA
tclean(vis='3c391_ctm_mosaic_spw0.ms',imagename='3c391_ctm_spw0_multiscale
    ',
      field='',spw='',
      specmode='mfs',
      niter=20000,
      gain=0.1, threshold='1.0mJy',
      gridder='mosaic',
      deconvolver='multiscale',
      scales=[0, 5, 15, 45], smallscalebias=0.9,
      interactive=True,
      imsize=[480,480], cell=['2.5arcsec','2.5arcsec'],
      stokes='I',
      weighting='briggs',robust=0.5,
      pbcor=False,
      savemodel='modelcolumn')
```

Task tclean is powerful with many inputs and a certain amount of experimentation likely is required.

We get the following image after running tclean for multiple iterations, until the residuals are uniform.

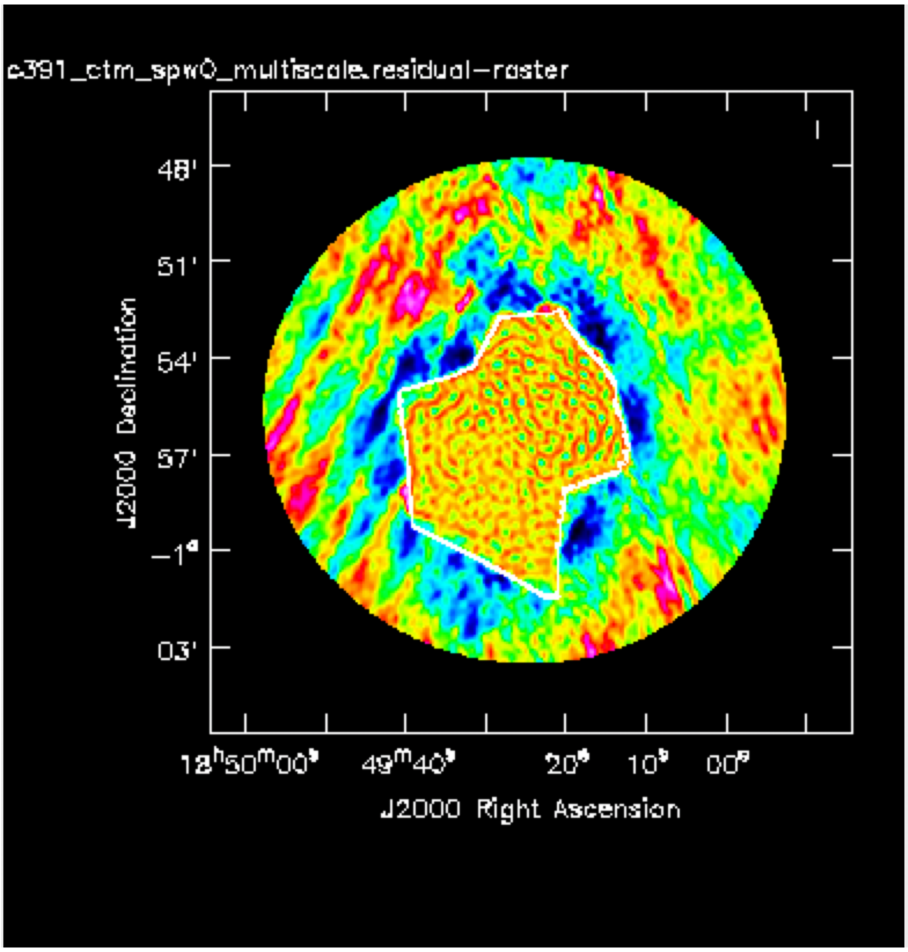

Figure 9.8: Supernova image after 15000+ iterations, until the residuals are uniform

After the imaging and deconvolution process has finished, we can use the viewer to look at your image.

```
    # In CASA
viewer(’3c391_ctm_spw0_multiscale.image’)
```

On running this,we get the following output:
The tclean task naturally operates in a flat noise image, i.e., an image where the effective weighting across the mosaic field of view is set so that the noise is constant. This is so that the clean threshold has a uniform meaning for the stopping criterion and that the image fed into the minor cycles has uniform noise levels. However, this means that the image does not take into account the primary beam fall-off in the edges and interstices of the mosaic. We could have set parameter pbcor=True in tclean, but it is useful to see the flat-noise image and residuals to evaluate the quality of the clean image. Therefore, we use impbcor to divide the .image by the .pb image to produce a primary beam corrected restored image:

```
    # In CASA
impbcor(imagename=’3c391_ctm_spw0_multiscale.image’,pbimage=’3
    c391_ctm_spw0_multiscale.pb’,
```

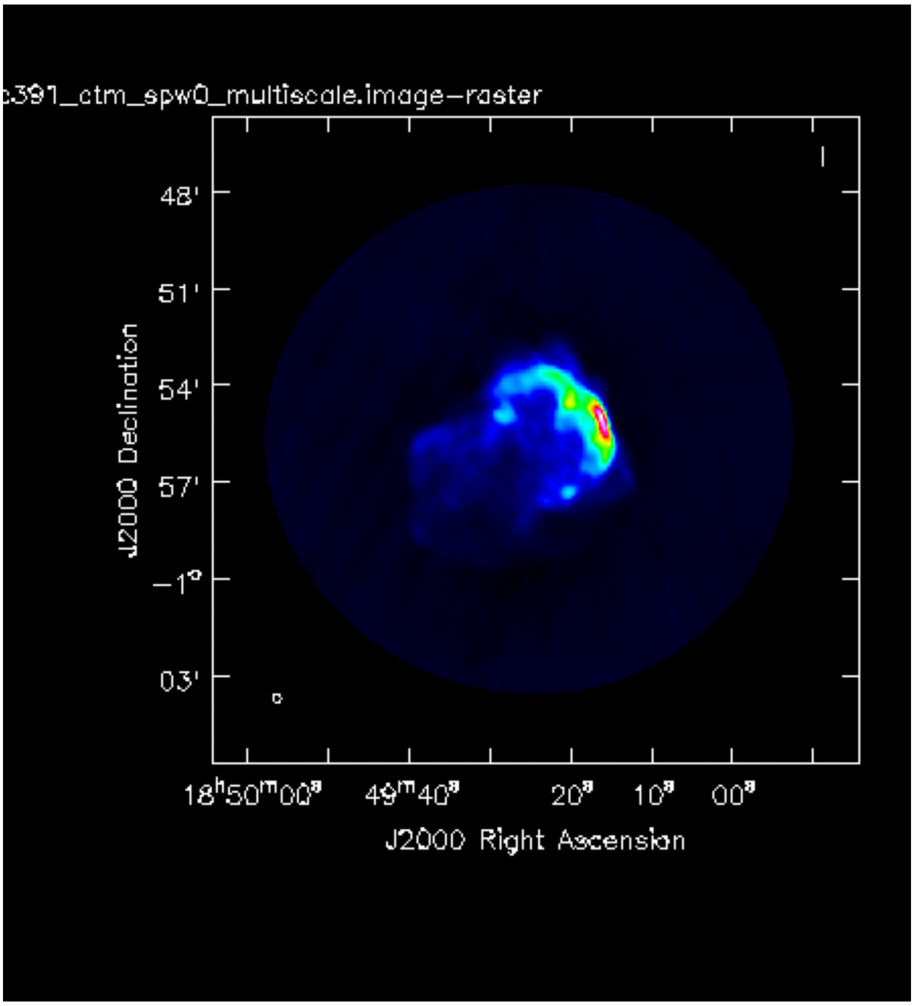
391_ctm_spw0_multiscale.image−raster
48'
51'
54'
57'
−1°
03'
J2000 Declination
18h50m00s
49m40s
20s
10s
00s
J2000 Right Ascension

Figure 9.9: Image of Super Nova after the interactive cleaning process

```
        outfile='3c391_ctm_spw0_multiscale.pbcorimage')
```

9.3.3 Image Analysis

The three most basic analyses are to determine the peak brightness, the flux density, and the image noise level. These are useful measures of how well the imaging efforts are in approaching the thermal noise limit or in reproducing what is already known about a source. Additional discussion of image analysis and manipulation, including the combination of multiple images, mathematical operations on images, and much more can be found in the Image Analysis section of the CASA documentation.
The most straightforward statistic is the peak brightness, which is determined by imstat.

```
    #IN CASA
    mystat = imstat(imagename='3c391_ctm_spw0_multiscale.pbcorimage')
```

Upon running this we get the final flux density to be **8.98 Jy**.

Below is the attached picture of the statistics

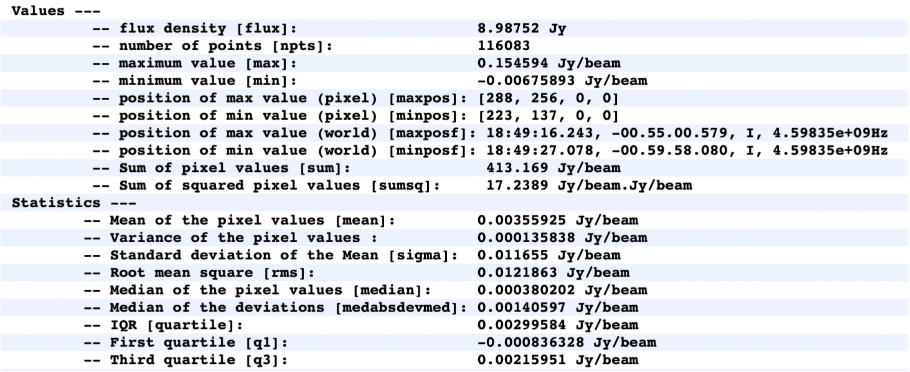

```
Values ---
         -- flux density [flux]:                    8.98752 Jy
         -- number of points [npts]:                116083
         -- maximum value [max]:                    0.154594 Jy/beam
         -- minimum value [min]:                    -0.00675893 Jy/beam
         -- position of max value (pixel) [maxpos]: [288, 256, 0, 0]
         -- position of min value (pixel) [minpos]: [223, 137, 0, 0]
         -- position of max value (world) [maxposf]: 18:49:16.243, -00.55.00.579, I, 4.59835e+09Hz
         -- position of min value (world) [minposf]: 18:49:27.078, -00.59.58.080, I, 4.59835e+09Hz
         -- Sum of pixel values [sum]:               413.169 Jy/beam
         -- Sum of squared pixel values [sumsq]:     17.2389 Jy/beam.Jy/beam
Statistics ---
        -- Mean of the pixel values [mean]:         0.00355925 Jy/beam
        -- Variance of the pixel values :           0.000135838 Jy/beam
        -- Standard deviation of the Mean [sigma]:  0.011655 Jy/beam
        -- Root mean square [rms]:                  0.0121863 Jy/beam
        -- Median of the pixel values [median]:     0.000380202 Jy/beam
        -- Median of the deviations [medabsdevmed]: 0.00140597 Jy/beam
        -- IQR [quartile]:                          0.00299584 Jy/beam
        -- First quartile [q1]:                     -0.000836328 Jy/beam
        -- Third quartile [q3]:                     0.00215951 Jy/beam
```

Figure 9.10: Supernova remnant Statistics

10. Markov-Chain Monte Carlo (MCMC)

MCMC (8) stands for Markov-Chain Monte Carlo, and it is a powerful method for fitting models to data. Unlike simple linear least squared or chi-squared fits, MCMC is a parameter space exploration tool, commonly known as a sampler.

The fundamental process of running an MCMC is to compare generated models against observed data. These models are generated based on a set of parameters, and the goal is to find the set of parameters that produces the model that best fits the observed data.

For the MCMC process to be feasible, it is inherently Bayesian, in contrast to the frequentist approach. Practically, this means that our MCMC requires us to impose what are known as priors on our parameters. These priors encode information that we, as modelers, think we already know about the system being modeled. For instance, if constructing a model for the sun, one might impose a prior that the temperature at the core falls within a certain range, based on observations that nuclear fusion occurs only above certain temperatures.

With the imposed priors, we then calculate the probability of our model given our data. The process typically involves exploring the parameter space using Markov chains, generating a range of models, and evaluating their likelihoods against the observed data to find the most probable set of parameters that best describe the system under study.

- **Establishing the Model-generating Function:**

  To fit models to data using the MCMC method, we first define a model-generating function that takes a set of input parameters and outputs a model. Let's consider a simple model that predicts the number of planets in an extrasolar system based on the host star's metallicity Z, mass M, and temperature T. The model-generating function can be represented as:

$$\text{Model}(Z, M, T) = \text{Number of Planets}$$

- **Ensemble of Walkers:**

  In the MCMC process, we create an ensemble of walkers, each defined by a θ vector that contains a set of parameters for the model-generating function. For our example, the θ_i vector corresponding to the i-th walker can be represented as:

  $$\theta_i = \begin{pmatrix} Z_i \\ M_i \\ T_i \end{pmatrix}$$

  We can imagine a "grid" of possible values for θ, within the prior ranges we've chosen to vary over.

- **Exploring the Parameter Space:**

  Each walker in the ensemble begins exploring the parameter space. It takes a "step" to a new value of θ and generates a model with that θ. It then compares the model to the given data using a simple χ^2-type check, calculating the "Likeness" as:

  $$\text{Likeness} = -\frac{1}{2}\sum\left(\frac{y_{\text{data}} - y_{\text{model}}}{y_{\text{data,err}}}\right)^2$$

  where y_{data} is the observed data, y_{model} is the model generated with θ, and $y_{\text{data,err}}$ is the data error.

- **MCMC Step and Parameter Update:**

  The MCMC then checks the ratio of the Likeness generated by the new model with the data to the Likeness of the previous model. If the new location produces a better match (higher Likeness), the walker moves there and repeats the process. If the new location is worse, it may still accept the move probabilistically to allow exploration of the parameter space.

- **Converging to High-Likeness Regions:**

  Over many iterations, the walkers begin to climb towards the regions of highest "likeness" between the models generated and the observed data. This process allows the MCMC to explore the parameter space and find the set of parameters that best fit the data, considering the priors we have imposed on the parameters.

At the end of the MCMC process, known as a production run, we obtain what is referred to as a posterior distribution or chain. Each walker in the ensemble keeps a record of every θ vector it explored during the process, along with the likelihood of the model given the data at that specific value of θ.

Through complex mathematical algorithms, which we won't delve into here, this distribution, assuming the MCMC has run long enough to converge reasonably (where the distribution of walkers stabilizes without significant changes as a function of step number), represents a sample of plausible models that can describe our data.

It's essential to remember that MCMC is a "sampler," not a "fitter." It does not pinpoint a single parameter set θ as the definitive "best" solution. Instead, one of our models may have the numerically highest value of "likeness" to the data, but running the MCMC again or continuing it for more iterations could yield different results. MCMC excels at providing information like "If you draw 100 random models from the posterior distribution, the spread in those models represents our ability to constrain the parameters within those models."

In essence, MCMC provides insights into the range of models that are consistent with the observed data and the associated uncertainties in the parameter estimates. This ensemble of models from the posterior distribution allows us to better understand the range of plausible solutions rather than a single "best" fit.

To understand this better, we evaluate one example:

10.0.1 Fitting the lightcurve of GW170817

In chapter 3, we had plotted the non-thermal jet emission in the radio and Xray band (VLA and Chandra, respectively). We will be attempting to do the same, but using MCMC techniques.

Light curves are graphical representations of the variation in brightness or flux of an astronomical object over time. Fitting light curves with models allows us to extract valuable information about the physical processes governing these sources. The smooth broken power-law model is one such model used to describe the flux evolution.

The smooth broken power-law model is parametrized as follows:

$$F(t,\nu) = \frac{2}{1}\left(\frac{\nu}{3\,\mathrm{GHz}}\right)^{\beta} \frac{F_p}{(t/t_p)^s} \left[\left(\frac{t}{t_p}\right)^{-s\alpha_1} + \left(\frac{t}{t_p}\right)^{-s\alpha_2}\right]^{-\frac{1}{s}}$$

where:
$F(t,\nu)$ is the flux density at time t and observing frequency ν.
β is the spectral index.
F_p is the flux density at 3 GHz at the light curve peak time t_p.
t is the time post-merger.
t_p is the light curve peak time.

s is the smoothness parameter.
α_1 and α_2 are the power-law rise and decay slopes, respectively.
On running the MCMC function, taking two frequencies (VLA 3G Hz and CHANDRA 2.41 x 10^{17} Hz, we get the following fit.

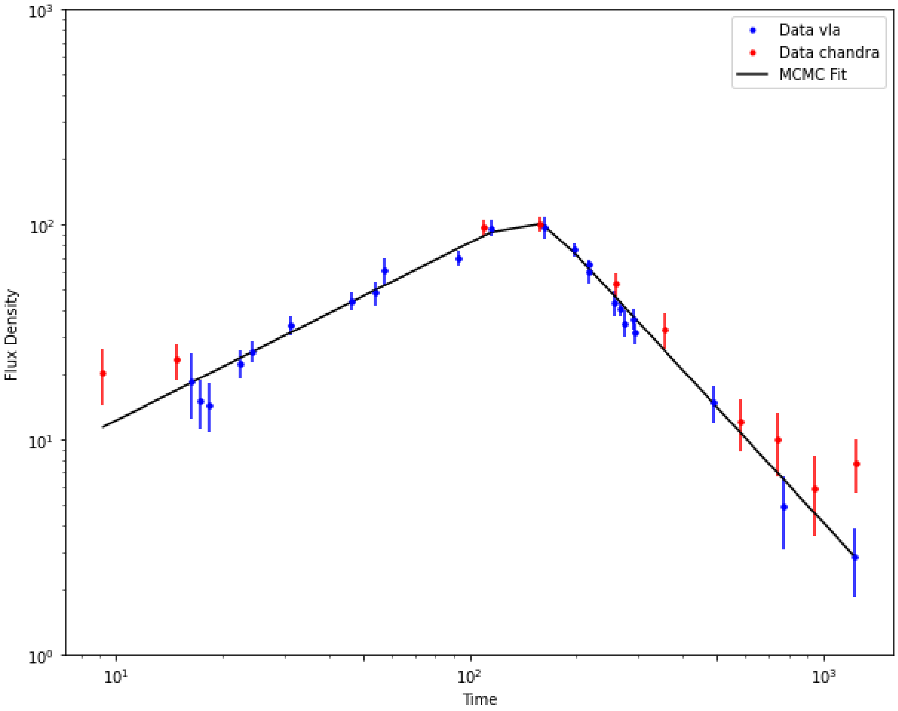

Figure 10.1: Broken power-law fit (using MCMC). *The light curve is scaled to 3 GHz utilizing the best-fit spectral index of -0.58 obtained from the MCMC analysis. The observed light curve exhibits a rising behavior with time as* $t^{0.86}$ *and a subsequent decline with time as* $t^{-1.72}$*. The peak of the light curve is observed at 158.84 days post-merger.*

Corner plots

Corner plots, also known as triangle plots, are graphical representations that offer valuable insights into the parameter space exploration and the posterior distribution obtained from the MCMC sampling.
Corner plots are particularly useful when dealing with multi-dimensional parameter spaces, where a model is fitted to data using multiple parameters. In such cases, visualizing the full parameter space can be challenging due to the high dimensionality. Corner plots address this challenge by providing a clear and intuitive way to examine the correlations and uncertainties among different parameters.
The corner plot displays a series of scatter plots, arranged in a triangle-like grid, with each scatter plot representing the relationship between two parameters. Along the diagonal of the grid, histograms show the marginal distributions of individual parameters.

Main features of corner plot are as follows:

Parameter Correlations: The scatter plots reveal the correlations between pairs

of parameters. If two parameters are correlated, their joint distribution will not be isotropic and may exhibit elongated or non-linear shapes in the scatter plot.
Parameter Covariances: By visually inspecting the joint distributions, it becomes easier to understand how changes in one parameter affect others. Covariance between parameters can indicate degeneracies, where different combinations of parameter values yield similar model fits to the data.
Uncertainty Estimation: The width and shape of the marginalized histograms along the diagonal provide insights into the uncertainties in individual parameters. The spread of the histogram indicates the range of plausible values for each parameter.
Identifying Multimodal Distributions: If the posterior distribution exhibits multiple modes (peaks), they may be visible as separate clusters or distinct features in the scatter plots.
Outliers and Model Fit: Corner plots allow researchers to identify outliers or unusual behavior in the parameter space that may impact the quality of the model fit.
As we saw, corner plots give the correlation between parameters. When we tried to obtain the corner plots for the lightcurves, we got this result:

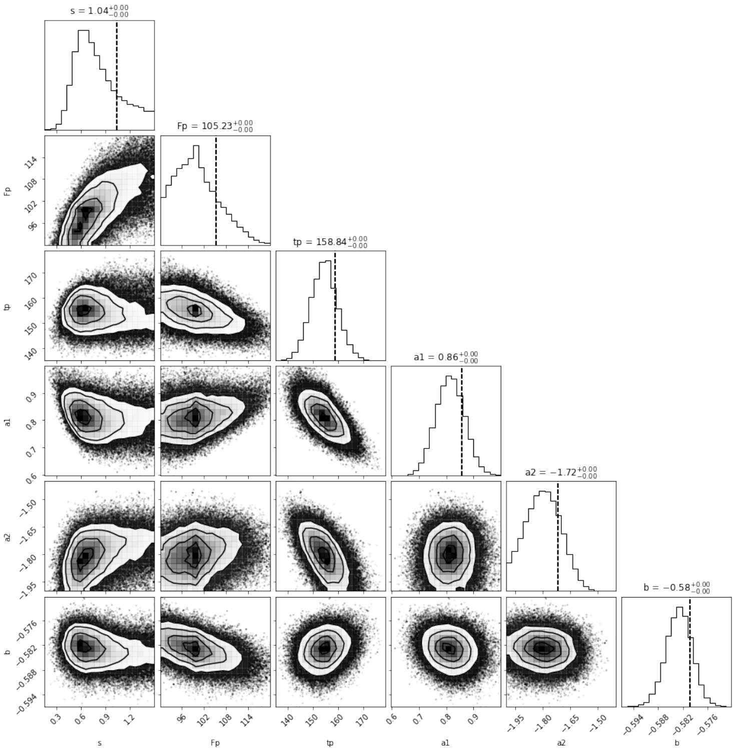

Figure 10.2: **Corner Plot for Broken Power-Law Fit:** *The corner plot showcases the parameter space exploration for the broken power-law fit to the light curve. The parameters b (spectral index), Fp (flux density at 3 GHz at light curve peak), tp (light curve peak time), a1 (power-law rise slope), and a2 (power-law decay slope) are analyzed to understand their correlations and likelihood distributions.*

The values and the plots are similar to the research paper(5) we were referring to, which proves that we got the correct plots and the correct values.

11. Fast Radio Bursts

Fast radio bursts (FRBs) are radio transients of millisecond duration and extragalactic origin.
The distribution of dispersion measure, DM, of Fast Radio Bursts (FRBs) from a given redshift z, $p(DM|z)$, is of significant interest in the study of FRBs. It provides insights into the propagation of radio waves through the intergalactic medium and the effects of dispersion caused by free electrons along the line of sight. Understanding this distribution is crucial for accurately interpreting the observed DM values and inferring the intrinsic properties of FRBs, such as their luminosities and distances.

In addition to its intrinsic interest, the distribution of DM is also a nuisance factor in analyzing the properties of the FRB population as a whole. The dispersion measure depends on the electron density along the path from the source to the observer, which can be affected by various astrophysical factors and intervening structures. This introduces uncertainties in the measured DM values and can complicate the statistical analysis and interpretation of FRB data.

Now, we will utilize data of a pulsar.
The different frequencies of the pulse from the Fast Radio Burst (FRB) arrive at different times, with the highest frequency coming first. This time delay, denoted as t_{arr}, is related to the Dispersion Measure (DM) and the observing frequency (ν) by the following equation:

$$t_{\text{arr}} \propto \text{DM} \times \nu^{-2}$$

Here, t_{arr} represents the time delay in seconds. The proportionality constant is given as 4.148808×10^{3} seconds, when the observing frequency ν is in MHz, and the Dispersion Measure DM is in pc cm^3 (pc - parsec is a unit of distance).

We will be using some data of a pulsar for this activity. The method is, however, the same for an FRB (Fast Radio Burst) also.
We start with the array dataset and Load it using numpy. Then we plot the 2d waterfall plot which comes out to be like this.

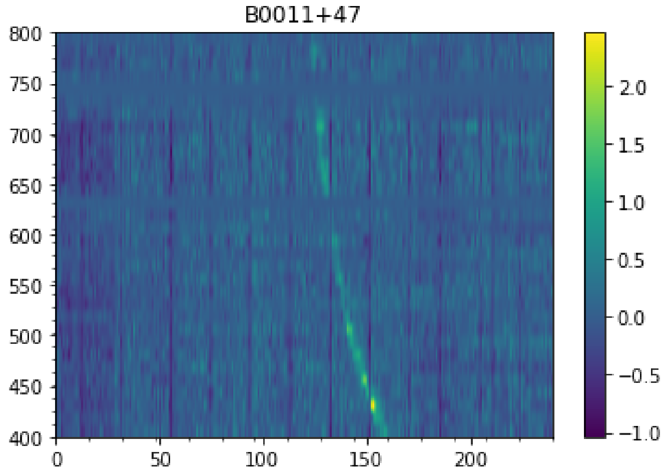

Figure 11.1: 2d Waterfall Plot: *Visualization of Array Dataset*

Using the delay calculated from the above equation, we attempt to shift the frequency channels of the data so that the pulse aligns properly.

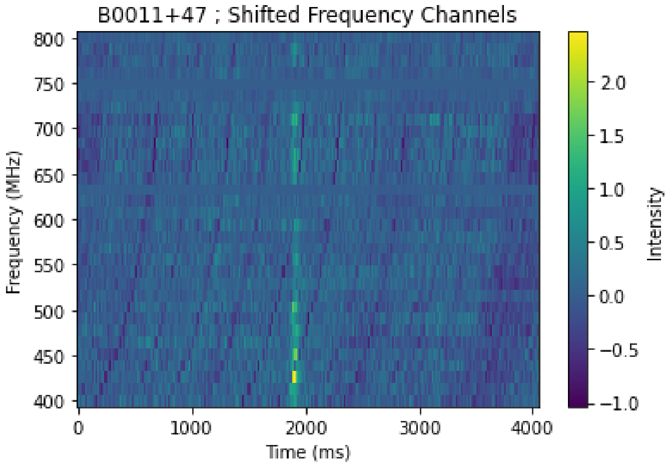

Figure 11.2: Lined-up Data Plot: Frequency Channels Aligned: *The frequency channels of the data have been appropriately shifted, resulting in a well-aligned pulse*

For calculating the time series, we sum over all frequency channels. We define a signal-to-noise ratio (SNR) for this time series by taking the ratio of the maximum of the absolute value of the time series to the mean of the absolute value of the time series.

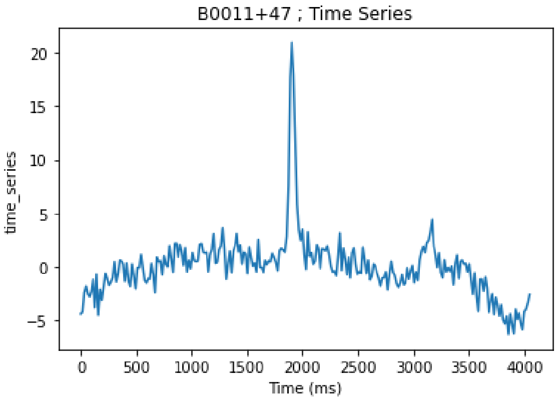

Figure 11.3: Time Series: *By finding the Dispersion Measure (DM) that maximizes the Signal-to-Noise Ratio (SNR), we effectively de-disperse the data, leading to a clear peak in the time series.*

We repeat this SNR calculation for many DMs and find the DM where SNR is maximum. This de-disperses the data and the best DM will give a nice peak in the time series.

On repeating this multiple times, we get our DM value to be 30.30 and our maximum SNR to be 7.45.

To help understand it better, I have plotted a DM vs SNR plot.

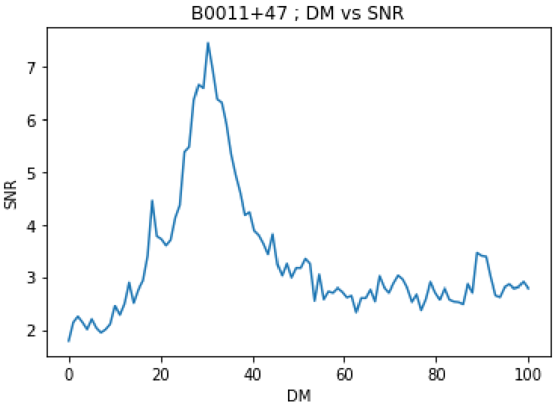

Figure 11.4: "Dispersion Measure (DM) vs. Signal-to-Noise Ratio (SNR)" *In this graph, we can observe how Dispersion Measure (DM) and Signal-to-Noise Ratio (SNR) are connected. The highest point on the plot appears at DM = 30.30, accompanied by an SNR value of 7.45.*

Bibliography

(1) LIGO Caltech. *GW170817 Press Release*. https://www.ligo.caltech.edu/page/press-release-gw170817.

(2) CIRADA. *CIRADA Cutouts*. http://cutouts.cirada.ca/help/.

(3) CASA Continuum. *VLA Continuum Tutorial 3C391-CASA6.4.1*. https://casaguides.nrao.edu/index.php?title=VLA_Continuum_Tutorial_3C391-CASA6.4.1.

(4) CASA Imaging. *CASA First Look at Imaging*. https://casaguides.nrao.edu/index.php?title=First_Look_at_Imaging_CASA_6.4.

(5) Sphesihle Makhathini et al. "The panchromatic afterglow of GW170817: the full uniform data set, modeling, comparison with previous results, and implications". In: *The Astrophysical Journal* 922.2 (2021), p. 154.

(6) J.M. Marr, R.L. Snell, and S.E. Kurtz. *Fundamentals of Radio Astronomy: Observational Methods*. Series in Astronomy and Astrophysics. CRC Press, 2015. ISBN: 9781498770194. URL: https://books.google.co.in/books?id=T54oCwAAQBAJ.

(7) John C Mather et al. "A preliminary measurement of the cosmic microwave background spectrum by the Cosmic Background Explorer (COBE) satellite". In: *Astrophysical Journal, Part 2-Letters (ISSN 0004-637X), vol. 354, May 10, 1990, p. L37-L40.* 354 (1990), pp. L37–L40.

(8) MCMC. *VLA Continuum Tutorial 3C391-CASA6.4.1*. https://prappleizer.github.io/Tutorials/MCMC/MCMC_Tutorial_Solution.html#So-what-is-MCMC?.

(9) European Southern Observatory. *Atacama Large Millimeter Array*. https://www.eso.org/public/teles-instr/alma/.

(10) Planck Satellite. *Cosmic Microwave Background*. https://plancksatellite.org.uk/science/cmb/.

(11) Hubble Site. *TW hydra*. https://hubblesite.org/contents/media/images/2013/20/3181-Image.html.